Amplitude Analysis and Branching Fraction Measurement of $D_s^+ \to K^+K^-\pi^+$

M. Ablikim[1], M. N. Achasov[10,d], S. Ahmed[15], M. Albrecht[4], M. Alekseev[55A,55C], A. Amoroso[55A,55C], F. F. An[1], Q. An[52,42], Y. Bai[41], O. Bakina[27], R. Baldini Ferroli[23A], Y. Ban[35], K. Begzsuren[25], D. W. Bennett[22], J. V. Bennett[5], N. Berger[26], M. Bertani[23A], D. Bettoni[24A], F. Bianchi[55A,55C], E. Boger[27,b], I. Boyko[27], R. A. Briere[5], H. Cai[57], X. Cai[1,42], A. Calcaterra[23A], G. F. Cao[1,46], S. A. Cetin[45B], J. Chai[55C], J. F. Chang[1,42], W. L. Chang[1,46], G. Chelkov[27,b,c], G. Chen[1], H. S. Chen[1,46], J. C. Chen[1], M. L. Chen[1,42], P. L. Chen[53], S. J. Chen[33], X. R. Chen[30], Y. B. Chen[1,42], W. Cheng[55C], X. K. Chu[35], G. Cibinetto[24A], F. Cossio[55C], H. L. Dai[1,42], J. P. Dai[37,h], A. Dbeyssi[15], D. Dedovich[27], Z. Y. Deng[1], A. Denig[26], I. Denysenko[27], M. Destefanis[55A,55C], F. De Mori[55A,55C], Y. Ding[31], C. Dong[34], J. Dong[1,42], L. Y. Dong[1,46], M. Y. Dong[1,42,46], Z. L. Dou[33], S. X. Du[60], P. F. Duan[1], J. Fang[1,42], S. S. Fang[1,46], Y. Fang[1], R. Farinelli[24A,24B], L. Fava[55B,55C], F. Feldbauer[4], G. Felici[23A], C. Q. Feng[52,42], M. Fritsch[4], C. D. Fu[1], Q. Gao[1], X. L. Gao[52,42], Y. Gao[44], Y. G. Gao[6], Z. Gao[52,42], B. Garillon[26], I. Garzia[24A], A. Gilman[49], K. Goetzen[11], L. Gong[34], W. X. Gong[1,42], W. Gradl[26], M. Greco[55A,55C], L. M. Gu[33], M. H. Gu[1,42], Y. T. Gu[13], A. Q. Guo[1], L. B. Guo[32], R. P. Guo[1,46], Y. P. Guo[26], A. Guskov[27], Z. Haddadi[29], S. Han[57], X. Q. Hao[16], F. A. Harris[47], K. L. He[1,46], X. Q. He[51], F. H. Heinsius[4], T. Held[4], Y. K. Heng[1,42,46], Z. L. Hou[1], H. M. Hu[1,46], J. F. Hu[37,h], T. Hu[1,42,46], Y. Hu[1], G. S. Huang[52,42], J. S. Huang[16], X. T. Huang[36], X. Z. Huang[33], Z. L. Huang[31], T. Hussain[54], W. Ikegami Andersson[56], M, Irshad[52,42], Q. Ji[1], Q. P. Ji[16], X. B. Ji[1,46], X. L. Ji[1,42], H. L. Jiang[36], X. S. Jiang[1,42,46], X. Y. Jiang[34], J. B. Jiao[36], Z. Jiao[18], D. P. Jin[1,42,46], S. Jin[33], Y. Jin[48], T. Johansson[56], A. Julin[49], N. Kalantar-Nayestanaki[29], X. S. Kang[34], M. Kavatsyuk[29], B. C. Ke[1,5,k], I. K. Keshk[4], T. Khan[52,42], A. Khoukaz[50], P. Kiese[26], R. Kiuchi[1], R. Kliemt[11], L. Koch[28], O. B. Kolcu[45B,f], B. Kopf[4], M. Kornicer[47], M. Kuemmel[4], M. Kuessner[4], A. Kupsc[56], M. Kurth[1], W. Kühn[28], J. S. Lange[28], P. Larin[15], L. Lavezzi[55C], S. Leiber[4], H. Leithoff[26], C. Li[56], Cheng Li[52,42], D. M. Li[60], F. Li[1,42], F. Y. Li[35], G. Li[1], H. B. Li[1,46], H. J. Li[1,46], J. C. Li[1], J. W. Li[40], K. J. Li[43], Kang Li[14], Ke Li[1], Lei Li[3], P. L. Li[52,42], P. R. Li[46,7], Q. Y. Li[36], T. Li[36], W. D. Li[1,46], W. G. Li[1], X. L. Li[36], X. N. Li[1,42], X. Q. Li[34], Z. B. Li[43], H. Liang[52,42], Y. F. Liang[39], Y. T. Liang[28], G. R. Liao[12], L. Z. Liao[1,46], J. Libby[21], C. X. Lin[43], D. X. Lin[15], B. Liu[37,h], B. J. Liu[1], C. X. Liu[1], D. Liu[52,42], D. Y. Liu[37,h], F. H. Liu[38], Fang Liu[1], Feng Liu[6], H. B. Liu[13], H. L Liu[41], H. M. Liu[1,46], Huanhuan Liu[1], Huihui Liu[17], J. B. Liu[52,42], J. Y. Liu[1,46], K. Y. Liu[31], Ke Liu[6], L. D. Liu[35], Q. Liu[46], S. B. Liu[52,42], X. Liu[30], Y. B. Liu[34], Z. A. Liu[1,42,46], Zhiqing Liu[26], Y. F. Long[35], X. C. Lou[1,42,46], H. J. Lu[18], J. G. Lu[1,42], Y. Lu[1], Y. P. Lu[1,42], C. L. Luo[32], M. X. Luo[59], P. W. Luo[43], T. Luo[9,j], X. L. Luo[1,42], S. Lusso[55C], X. R. Lyu[46], F. C. Ma[31], H. L. Ma[1], L. L. Ma[36], M. M. Ma[1,46], Q. M. Ma[1], X. N. Ma[34], X. Y. Ma[1,42], Y. M. Ma[36], F. E. Maas[15], M. Maggiora[55A,55C], S. Maldaner[26], Q. A. Malik[54], A. Mangoni[23B], Y. J. Mao[35], Z. P. Mao[1], S. Marcello[55A,55C], Z. X. Meng[48], J. G. Messchendorp[29], G. Mezzadri[24A], J. Min[1,42], T. J. Min[33], R. E. Mitchell[22], X. H. Mo[1,42,46], Y. J. Mo[6], C. Morales Morales[15], N. Yu. Muchnoi[10,d], H. Muramatsu[49], A. Mustafa[4], S. Nakhoul[11,g], Y. Nefedov[27], F. Nerling[11,g], I. B. Nikolaev[10,d], Z. Ning[1,42], S. Nisar[8], S. L. Niu[1,42], X. Y. Niu[1,46], S. L. Olsen[46], Q. Ouyang[1,42,46], S. Pacetti[23B], Y. Pan[52,42], M. Papenbrock[56], P. Patteri[23A], M. Pelizaeus[4], J. Pellegrino[55A,55C], H. P. Peng[52,42], Z. Y. Peng[13], K. Peters[11,g], J. Pettersson[56], J. L. Ping[32], R. G. Ping[1,46], A. Pitka[4], R. Poling[49], V. Prasad[52,42], H. R. Qi[2], M. Qi[33], T. Y. Qi[2], S. Qian[1,42], C. F. Qiao[46], N. Qin[57], X. S. Qin[4], Z. H. Qin[1,42], J. F. Qiu[1], S. Q. Qu[34], K. H. Rashid[54,i], C. F. Redmer[26], M. Richter[4], M. Ripka[26], A. Rivetti[55C], M. Rolo[55C], G. Rong[1,46], Ch. Rosner[15], A. Sarantsev[27,e], M. Savrié[24B], K. Schoenning[56], W. Shan[19], X. Y. Shan[52,42], M. Shao[52,42], C. P. Shen[2], P. X. Shen[34], X. Y. Shen[1,46], H. Y. Sheng[1], X. Shi[1,42], J. J. Song[36], W. M. Song[36], X. Y. Song[1], S. Sosio[55A,55C], C. Sowa[4], S. Spataro[55A,55C], F. F. Sui[36], G. X. Sun[1], J. F. Sun[16], L. Sun[57], S. S. Sun[1,46], X. H. Sun[1], Y. J. Sun[52,42], Y. K Sun[52,42], Y. Z. Sun[1], Z. J. Sun[1,42], Z. T. Sun[1], Y. T Tan[52,42], C. J. Tang[39], G. Y. Tang[1], X. Tang[1], M. Tiemens[29], B. Tsednee[25], I. Uman[45D], B. Wang[1], B. L. Wang[46], C. W. Wang[33], D. Wang[35], D. Y. Wang[35], Dan Wang[46], H. H. Wang[36], K. Wang[1,42], L. L. Wang[1], L. S. Wang[1], M. Wang[36], Meng Wang[1,46], P. Wang[1], P. L. Wang[1], W. P. Wang[52,42], X. F. Wang[1], Y. Wang[52,42], Y. F. Wang[1,42,46], Z. Wang[1,42], Z. G. Wang[1,42], Z. Y. Wang[1], Zongyuan Wang[1,46], T. Weber[4], D. H. Wei[12], P. Weidenkaff[26], S. P. Wen[1], U. Wiedner[4], M. Wolke[56], L. H. Wu[1], L. J. Wu[1,46], Z. Wu[1,42], L. Xia[52,42], X. Xia[36], Y. Xia[20], D. Xiao[1], Y. J. Xiao[1,46], Z. J. Xiao[32], Y. G. Xie[1,42], Y. H. Xie[6], X. A. Xiong[1,46], Q. L. Xiu[1,42], G. F. Xu[1], J. J. Xu[1,46], L. Xu[1], Q. J. Xu[14], X. P. Xu[40], F. Yan[53], L. Yan[55A,55C], W. B. Yan[52,42], W. C. Yan[2], Y. H. Yan[20], H. J. Yang[37,h], H. X. Yang[1], L. Yang[57], R. X. Yang[52,42], S. L. Yang[1,46], Y. H. Yang[33], Y. X. Yang[12], Yifan Yang[1,46], Z. Q. Yang[20], M. Ye[1,42], M. H. Ye[7], J. H. Yin[1], Z. Y. You[43], B. X. Yu[1,42,46], C. X. Yu[34], J. S. Yu[20], J. S. Yu[30], C. Z. Yuan[1,46], Y. Yuan[1], A. Yuncu[45B,a], A. A. Zafar[54], Y. Zeng[20], B. X. Zhang[1], B. Y. Zhang[1,42], C. C. Zhang[1], D. H. Zhang[1], H. H. Zhang[43], H. Y. Zhang[1,42], J. Zhang[1,46], J. L. Zhang[58], J. Q. Zhang[4], J. W. Zhang[1,42,46], J. Y. Zhang[1], J. Z. Zhang[1,46], K. Zhang[1,46], L. Zhang[44], S. F. Zhang[33], T. J. Zhang[37,h], X. Y. Zhang[36], Y. Zhang[52,42], Y. H. Zhang[1,42], Y. T. Zhang[52,42], Yang Zhang[1], Yao Zhang[1], Yu Zhang[46], Z. H. Zhang[6], Z. P. Zhang[52], Z. Y. Zhang[57], G. Zhao[1], J. W. Zhao[1,42], J. Y. Zhao[1,46], J. Z. Zhao[1,42], Lei Zhao[52,42], Ling Zhao[1], M. G. Zhao[34], Q. Zhao[1], S. J. Zhao[60], T. C. Zhao[1], Y. B. Zhao[1,42], Z. G. Zhao[52,42], A. Zhemchugov[27,b], B. Zheng[53], J. P. Zheng[1,42], W. J. Zheng[36], Y. H. Zheng[46], B. Zhong[32], L. Zhou[1,42], Q. Zhou[1,46], X. Zhou[57], X. K. Zhou[52,42], X. R. Zhou[52,42], X. Y. Zhou[1], Xiaoyu Zhou[20], Xu Zhou[20], A. N. Zhu[1,46], J. Zhu[34], J. Zhu[43], K. Zhu[1], K. J. Zhu[1,42,46], S. Zhu[1], S. H. Zhu[51], X. L. Zhu[44], Y. C. Zhu[52,42], Y. S. Zhu[1,46], Z. A. Zhu[1,46], J. Zhuang[1,42], B. S. Zou[1], J. H. Zou[1]

(BESIII Collaboration)

[1] Institute of High Energy Physics, Beijing 100049, People's Republic of China
[2] Beihang University, Beijing 100191, People's Republic of China
[3] Beijing Institute of Petrochemical Technology, Beijing 102617, People's Republic of China
[4] Bochum Ruhr-University, D-44780 Bochum, Germany
[5] Carnegie Mellon University, Pittsburgh, Pennsylvania 15213, USA

[6] *Central China Normal University, Wuhan 430079, People's Republic of China*
[7] *China Center of Advanced Science and Technology, Beijing 100190, People's Republic of China*
[8] *COMSATS Institute of Information Technology, Lahore, Defence Road, Off Raiwind Road, 54000 Lahore, Pakistan*
[9] *Fudan University, Shanghai 200443, People's Republic of China*
[10] *G.I. Budker Institute of Nuclear Physics SB RAS (BINP), Novosibirsk 630090, Russia*
[11] *GSI Helmholtzcentre for Heavy Ion Research GmbH, D-64291 Darmstadt, Germany*
[12] *Guangxi Normal University, Guilin 541004, People's Republic of China*
[13] *Guangxi University, Nanning 530004, People's Republic of China*
[14] *Hangzhou Normal University, Hangzhou 310036, People's Republic of China*
[15] *Helmholtz Institute Mainz, Johann-Joachim-Becher-Weg 45, D-55099 Mainz, Germany*
[16] *Henan Normal University, Xinxiang 453007, People's Republic of China*
[17] *Henan University of Science and Technology, Luoyang 471003, People's Republic of China*
[18] *Huangshan College, Huangshan 245000, People's Republic of China*
[19] *Hunan Normal University, Changsha 410081, People's Republic of China*
[20] *Hunan University, Changsha 410082, People's Republic of China*
[21] *Indian Institute of Technology Madras, Chennai 600036, India*
[22] *Indiana University, Bloomington, Indiana 47405, USA*
[23] *(A)INFN Laboratori Nazionali di Frascati, I-00044, Frascati, Italy; (B)INFN and University of Perugia, I-06100, Perugia, Italy*
[24] *(A)INFN Sezione di Ferrara, I-44122, Ferrara, Italy; (B)University of Ferrara, I-44122, Ferrara, Italy*
[25] *Institute of Physics and Technology, Peace Ave. 54B, Ulaanbaatar 13330, Mongolia*
[26] *Johannes Gutenberg University of Mainz, Johann-Joachim-Becher-Weg 45, D-55099 Mainz, Germany*
[27] *Joint Institute for Nuclear Research, 141980 Dubna, Moscow region, Russia*
[28] *Justus-Liebig-Universitaet Giessen, II. Physikalisches Institut, Heinrich-Buff-Ring 16, D-35392 Giessen, Germany*
[29] *KVI-CART, University of Groningen, NL-9747 AA Groningen, The Netherlands*
[30] *Lanzhou University, Lanzhou 730000, People's Republic of China*
[31] *Liaoning University, Shenyang 110036, People's Republic of China*
[32] *Nanjing Normal University, Nanjing 210023, People's Republic of China*
[33] *Nanjing University, Nanjing 210093, People's Republic of China*
[34] *Nankai University, Tianjin 300071, People's Republic of China*
[35] *Peking University, Beijing 100871, People's Republic of China*
[36] *Shandong University, Jinan 250100, People's Republic of China*
[37] *Shanghai Jiao Tong University, Shanghai 200240, People's Republic of China*
[38] *Shanxi University, Taiyuan 030006, People's Republic of China*
[39] *Sichuan University, Chengdu 610064, People's Republic of China*
[40] *Soochow University, Suzhou 215006, People's Republic of China*
[41] *Southeast University, Nanjing 211100, People's Republic of China*
[42] *State Key Laboratory of Particle Detection and Electronics, Beijing 100049, Hefei 230026, People's Republic of China*
[43] *Sun Yat-Sen University, Guangzhou 510275, People's Republic of China*
[44] *Tsinghua University, Beijing 100084, People's Republic of China*
[45] *(A)Ankara University, 06100 Tandogan, Ankara, Turkey; (B)Istanbul Bilgi University, 34060 Eyup, Istanbul, Turkey; (C)Uludag University, 16059 Bursa, Turkey; (D)Near East University, Nicosia, North Cyprus, Mersin 10, Turkey*
[46] *University of Chinese Academy of Sciences, Beijing 100049, People's Republic of China*
[47] *University of Hawaii, Honolulu, Hawaii 96822, USA*
[48] *University of Jinan, Jinan 250022, People's Republic of China*
[49] *University of Minnesota, Minneapolis, Minnesota 55455, USA*
[50] *University of Muenster, Wilhelm-Klemm-Str. 9, 48149 Muenster, Germany*
[51] *University of Science and Technology Liaoning, Anshan 114051, People's Republic of China*
[52] *University of Science and Technology of China, Hefei 230026, People's Republic of China*
[53] *University of South China, Hengyang 421001, People's Republic of China*
[54] *University of the Punjab, Lahore-54590, Pakistan*
[55] *(A)University of Turin, I-10125, Turin, Italy; (B)University of Eastern Piedmont, I-15121, Alessandria, Italy; (C)INFN, I-10125, Turin, Italy*
[56] *Uppsala University, Box 516, SE-75120 Uppsala, Sweden*
[57] *Wuhan University, Wuhan 430072, People's Republic of China*
[58] *Xinyang Normal University, Xinyang 464000, People's Republic of China*
[59] *Zhejiang University, Hangzhou 310027, People's Republic of China*
[60] *Zhengzhou University, Zhengzhou 450001, People's Republic of China*

[a] *Also at Bogazici University, 34342 Istanbul, Turkey*
[b] *Also at the Moscow Institute of Physics and Technology, Moscow 141700, Russia*
[c] *Also at the Functional Electronics Laboratory, Tomsk State University, Tomsk, 634050, Russia*
[d] *Also at the Novosibirsk State University, Novosibirsk, 630090, Russia*
[e] *Also at the NRC "Kurchatov Institute", PNPI, 188300, Gatchina, Russia*

[f] *Also at Istanbul Arel University, 34295 Istanbul, Turkey*

[g] *Also at Goethe University Frankfurt, 60323 Frankfurt am Main, Germany*

[h] *Also at Key Laboratory for Particle Physics, Astrophysics and Cosmology, Ministry of Education; Shanghai Key Laboratory for Particle Physics and Cosmology; Institute of Nuclear and Particle Physics, Shanghai 200240, People's Republic of China*

[i] *Also at Government College Women University, Sialkot - 51310. Punjab, Pakistan.*

[j] *Also at Key Laboratory of Nuclear Physics and Ion-beam Application (MOE) and Institute of Modern Physics, Fudan University, Shanghai 200443, People's Republic of China*

[k] *Also at Shanxi Normal University, Linfen 041004, People's Republic of China*

(Dated: January 16, 2020)

We report the amplitude analysis and branching fraction measurement of $D_s^+ \to K^+ K^- \pi^+$ decay using a data sample of 3.19 fb^{-1} recorded with BESIII detector at a center-of-mass energy of 4.178 GeV. We perform a model-independent partial wave analysis (MIPWA) in the low $K^+ K^-$ region to extract the $K^+ K^-$ S-wave lineshape. We also perform an amplitude analysis on a nearly background free sample of 4399 events to investigate the substructure, and determine the relative fractions and the phases among the different intermediate processes. The amplitude analysis results provide an accurate detection efficiency and allow us to measure the branching fraction of $D_s^+ \to K^+ K^- \pi^+$ to be $\mathcal{B}(D_s^+ \to K^+ K^- \pi^+) = (5.47 \pm 0.08_{stat.} \pm 0.13_{sys.})\%$.

I. INTRODUCTION

Knowledge of the substructures in $D_s^+ \to K^+ K^- \pi^+$ decay allows us to properly determine the detection efficiency when measuring its branching fraction. Dalitz plot analyses of this decay have been performed by the E687 [1], CLEO [2] and Babar [3] collaborations. E687 used about 700 events and did not take $f_0(1370)\pi^+$ into account. For CLEO-c, about 14400 events with purity about 84.9% were selected with the single tag method. The analysis of BARBAR used about 100000 events with purity about 95%. Table I shows the comparision of the fitted decay fractions with the Dalitz plot analyses of previous analyses. From Table I, we can see an obvious difference of decay fraction of $S(980)\pi^+$ between BABAR and CLEO-c. Here S(980) denotes the $a_0(980)$ and $f_0(980)$ resonances. In this analysis with the double tag method, we can get a nearly background free data sample, which is good to perform the amplitude analysis.

In addition, experimental measurements can help to refine theoretical models [5]. Table II shows the predictions of the branching fractions of $D_s^+ \to \bar{K}^*(892)^0 K^+$ and $D_s^+ \to \phi(1020)\pi^+$, which can be obtained according to this analysis.

II. BESIII DETECTOR AND DATA SETS

The BESIII detector is a magnetic spectrometer [6] located at the Beijing Electron Positron Collider (BEPCII) [7]. The subdetectors surrounded by the superconducting solenoidal magnet, which provide a 1.0 T magnetic field, starting from the interaction point consist of a main drift chamber (MDC), a plastic scintillator time of flight counters (TOF), a CsI(Tl) electromagnetic calorimeter (EMC). Charged particle identification is performed by combining the ionization energy loss measured by MDC and the time-of-flight measured by TOF. EMC provides the shower information to reconstruct photons. Outside the solenoidal magnet is a multigap resistive-plate chamber system (MRPC), which provides muon identification.

Monte Carlo (MC) samples are produced with the GEANT4-based [8] package. An inclusive MC sample is produced at $E_{cm} = 4.178$ GeV. The sample includes all known open charm decays, the continuum processes ($e^+ e^- \to q\bar{q}$, q = u, d and s), Bhabha scattering, $\mu^+ \mu^-$, $\tau^+ \tau^-$, diphoton process and the $c\bar{c}$ resonances J/ψ, $\psi(3686)$ and $\psi(3770)$ via the initial state radiation (ISR). The generator CONEXC [9] is used to model the open charm processes directly produced via $e^+ e^-$ annihilation. The simulation of ISR production of $\psi(3770)$, $\psi(3686)$ and J/ψ is performed with the KKMC [10] package. The final-state radiation from charged tracks is produced by the PHOTOS package [11]. The known decays with BFs taken from Particle Data Group (PDG) [12] are simulated with the EVTGEN package [13] and the unknown decays are generated with the LUNDCHARM model [15]. The inclusive MC (generic MC) is used to perform background analysis.

III. EVENT SELECTION

For charged tracks except for those from K_S^0 decays, the polar angles (θ) respect to the beam axis must sat-

TABLE I. Comparison between Babar, CLEO-c and E687 Dalitz plot analysis.

Decay mode	Fit fraction(BABAR)	Fit fraction(CLEO-c)	Fit fraction(E687)
$D_s^+ \to \bar{K}^*(892)^0 K^+$	47.9±0.5±0.5	47.4±1.5±0.4	47.8±4.6±4.0
$D_s^+ \to \phi(1020)\pi^+$	41.4±0.8±0.5	42.2±1.6±0.3	39.6±3.3±4.7
$D_s^+ \to S(980)\pi^+$	16.4±0.7±2.0	28.2±1.9±1.8	11.0±3.5±2.6
$D_s^+ \to \bar{K}_0^*(1430)^0 K^+$	2.4±0.3±1.0	3.9±0.5±0.5	9.3±3.2±3.2
$D_s^+ \to f_0(1710)\pi^+$	1.1±0.1±0.1	3.4±0.5±0.3	3.4±2.3±3.5
$D_s^+ \to f_0(1370)\pi^+$	1.1±0.1±0.2	4.3±0.6±0.5	...
$\sum FF(\%)$	110.2±0.6±2.0	129.5±4.4±2.0	111.1
χ^2/NDF	$\frac{2843}{2305-14} = 1.2$	$\frac{178}{117} = 1.5$	$\frac{50.2}{33} = 1.5$
Events	96307 ± 369	12226 ± 22	701 ± 36

TABLE II. $\mathcal{B}(A1)$, $\mathcal{B}(S4)$, $\mathcal{B}(pole)$ and $\mathcal{B}(FAT[mix])$ are 4 theory predictions [5].

Mode	$\mathcal{B}(A1)$ (%)	$\mathcal{B}(S4)$ (%)	$\mathcal{B}(pole)$ (%)	$\mathcal{B}(FAT[mix])$ (%)
$D_s^+ \to \bar{K}^*(892)^0 K^+$	3.92 ± 1.13	3.93 ± 1.10	4.2 ± 1.7	4.07
$D_s^+ \to \phi(1020)\pi^+$	4.49 ± 0.40	4.51 ± 0.43	4.3 ± 0.6	3.4

isfy $|cos\theta| < 0.93$. The distances of charged tracks from the interaction point in the transverse plane and along the beam direction should be less than 1 cm and 10 cm, respectively.

Photons are reconstructed from the cluster shower in EMC. The deposit energy of the photons from the endcap ($0.86 < |cos\theta| < 0.92$) should be larger than 50 MeV and that of the photons from the barrel ($|cos\theta| < 0.8$) should be larger than 25 MeV. Furthermore, the shower time from the event start time should be within 700 ns.

We reconstruct $\pi^0(\eta)$ candidates through $\pi^0 \to \gamma\gamma$ ($\eta \to \gamma\gamma$). The diphoton invariant mass $M_{\gamma\gamma}$ for π^0 and η should be in the range of $0.115 < M_{\gamma\gamma} < 0.150$ GeV/c^2 and $0.490 < M_{\gamma\gamma} < 0.580$ GeV/c^2, respectively. Then we perform a fit to constrain $M_{\gamma\gamma}$ to the π^0 or η nominal mass [12]. The π^0 or η candidates with a χ_{1C}^2 less than 30 are retained.

Kaons and pions are identified by the combining the information of dE/dx in the MDC and the time-of-flight from the TOF. If the probability of the kaon hypothesis is larger than that of the pion hypothesis, the charged track is identified as a kaon. Otherwise, the track is identified as a pion.

We vote the $\pi^\pm$ and pi^0 whose momentum is less than 0.1 GeV to remove soft $\pi^\pm$ and π^0 from D^* decays.

The $\eta^{'}$ candidates are reconstructed via the process $\eta^{'} \to \pi^+\pi^-\eta$. The candidates with an invariant mass for $\pi^+\pi^-\eta$ falling into the range of $[0.938, 0.978]$ GeV/c^2 are retained.

$\pi^+\pi^-$ pairs are used to reconstruct K_S^0 mesons. The polar angles θ of the two pions should satisfy $|cos\theta| < 0.93$. The distances of the two pions should from the interaction point along the beam direction should be less

than 20 cm. The invariant mass $M(\pi^+\pi^-)$ of $\pi^+\pi^-$ pairs should satisfy $0.487 < M(\pi^+\pi^-) < 0.511$ GeV/c^2. The decay length and the decay length error of K_S^0 are obtained with second vertex fit. We require the decay length over the decay length error to be less than 2.

Then the D_s candidates are reconstructed from $K^\pm$, $\pi^\pm$, η, $\eta^{'}$, K_S^0 and π^0. We reserve the candidates with an invariant mass $M(D_s)$ falling in the mass window $[1.87, 2.06]$ GeV/c^2 and an recoiling mass M_{rec} falling in the mass window $[2.051, 2.180]$ GeV/c^2. M_{rec} is defined as:

$$M_{rec} = \sqrt{(E_{cm} - \sqrt{|\vec{p}_{D_s}|^2 + m_{D_s}^2})^2 - |\vec{p}_{cm} - \vec{p}_{D_s}|^2} ,$$
(1)

where p_{D_s} is the momentum of D_s candidate, m_{D_s} is D_s mass quoted from PDG [12], and $\vec{p}_{cm}$ and $\vec{p}_{D_s}$ are the momentum of the initial state and the decay products of the D_s candidate, respectively.

IV. PARTIAL WAVE ANALYSIS IN THE LOW K^+K^- MASS REGION

As it's very hard to distinguish $a_0(980)$ and $f_0(980)$ in the low K^+K^- mass region, we use S(980) to denote the $a_0(980)$ and $f_0(980)$ resonances and we perform a model-independent partial wave analysis (MIPWA) to extract S(980) line shape near the threshold of K^+K^- mass spectrum.

After the selection in Sec. III, for each D_s candidates decaying to $K^+K^-\pi^+$ in an event, all daughter tracks are added to apply a 1C kinematic fit constraining the mass of D_s. Then we select the can-

didate with minimum χ^2_{1C} as the best candidate in an event. We define the invariant mass of the D_s with opposite charge to the signal D_s as $M_{oth} = \sqrt{(E_{cm} - \sqrt{|\vec{p}_{D_s}|^2 + m_{D_s}} - E_\gamma)^2 - |\vec{p}_{cm} - \vec{p}_{D_s} - \vec{p}_\gamma|^2}$, where E_γ and $\vec{p}_\gamma$ refer to the energy and momentum of gamma from the process $D_s^* \to D_s\gamma$. The good gamma with M_{oth} closest to the nominal D_s mass [12] is taken as the gamma from the decay $D_s^* \to D_s\gamma$.

Multi-variable analysis (MVA) method [14] is used to suppress the background. With the gradient boosted decision tree (BDTG) classifier provided by MVA, we train MVA separately with two sets of variables for the two categories depending on the D_s^+ origin. Two categories of events are selected in a $M_{rec} - \Delta M$ 2D plane, where $\Delta M \equiv M(D_s^+\gamma) - M(D_s^+)$, $M(D_s^+)$ is the invariant mass of signal D_s and $M(D_s^+\gamma)$ refers to the invariant mass of D_s and the gamma from $D_s^* \to D_s\gamma$, as shown in Fig. 1.
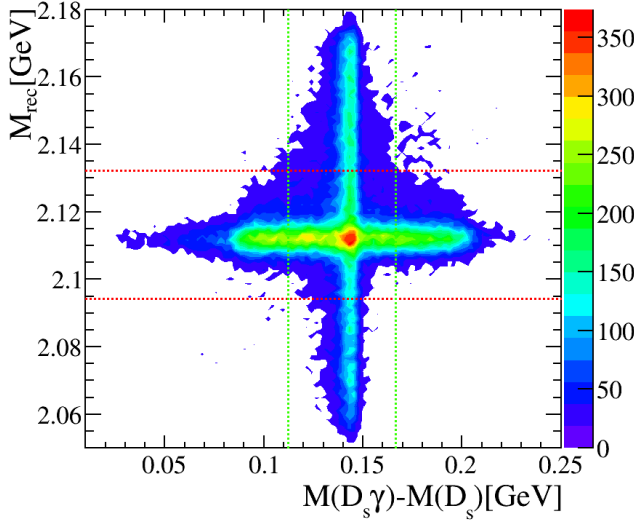

FIG. 1. Two dimensional plane of M_{rec} versus $\Delta M \equiv M(D_s^+\gamma) - M(D_s^+)$ from the simulated $D_s^+ \to K^+K^-\pi^+$ decays. The red (green) dashed lines mark the mass window for the D_s^+ Cat. #0 (Cat. #1) around the M_{rec} (ΔM) peak.

For Cat. #0, the BDTG takes three discriminating variables as input: the recoiling mass M_{rec}, the total momentum of the tracks and neutrals in the rest of event (not part of the $D_s^+ \to K^+K^-\pi^+$ candidate) and the energy of gamma from D_s^* E_γ. We define M'_{rec} as $M'_{rec} = \sqrt{\left(E_{cm} - \sqrt{p_{D_s\gamma}^2 + m_{D_s^*}^2}\right)^2 - p_{D_s\gamma}^2}$, with $p_{D_s\gamma}$ as the momentum of the $D_s\gamma$ combination, $m_{D_s^*}$ as the nominal D_s^* mass. For Cat. #1, the BDTG takes another three variables as input: ΔM, M'_{rec} and the total number of tracks and neutrals in an event N_{tracks}. According to the studies of generic MC, with the BDTG cut criteria, we can get a relatively pure sample (background less than 4%) and the background ratios of Cat.# 0 and Cat.#1

are almost the same. After applying the BDTG requirement, the fit to the signal D_s invariant mass gives the background yield in signal region ($1.95 < M(D_s) < 1.986$ GeV/c^2) is 735.7 ± 30.0 and the corresponding signal yield is 18590.6 ± 141.0, shown as in Fig. 2. In the fit, the signal shape is modeled with the MC-simulated shape convoluted with a Gaussian function and the background is described with a second-order Chebychev polynomial.
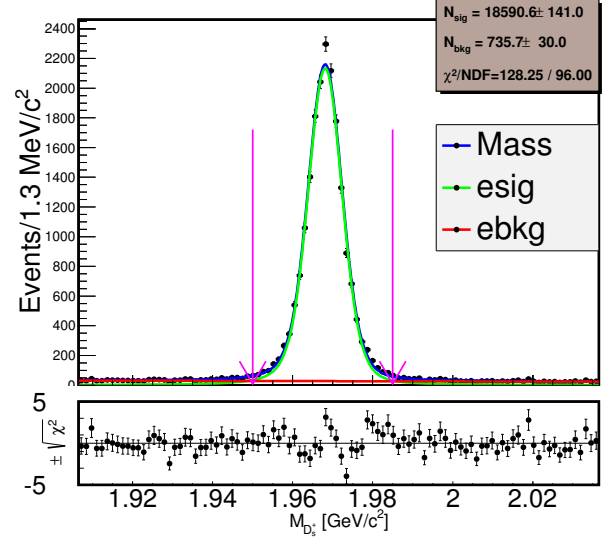

FIG. 2. The fit to the signal D_s invariant mass (M_{D_s}) spectrum (the dots with error bars) after BDTG requirement, the area between the pink arrows is the signal area of the sample for MIPWA. The signal shape (green line) is the MC shape convoluted with a Gaussian function and the background shape (red line) is second-order Chebychev polynomial.

Assuming N is the number of events for a given mass interval, the angular distributions $\frac{dN}{d\cos\Theta}$ can be expanded in terms of harmonic functions:

$$\frac{dN}{d\cos\Theta} = 2\pi \sum_{k=0}^{L_{max}} \langle Y_k^0 \rangle Y_k^0(\cos\Theta), \qquad (2)$$

where $L_{max} = 2\ell_{max}$, and ℓ_{max} is the maximum orbital angular momentum quantum number required to describe the K^+K^- system at $m_{K^+K^-}$ (e.g. $\ell_{max} = 1$ for S-, P-wave description); Θ is the angle between the K^+ direction in the K^+K^- rest frame and the prior direction of the K^+K^- system in the D_s^+ rest frame, $Y_k^0(\cos\Theta) = \sqrt{(2k+1)/4\pi}P_k(cos\Theta)$ are harmonic functions, $P_k(cos\Theta)$ is k-th order Legendre polynomial. $\frac{dN}{d\cos\Theta}$ has been efficiency corrected, phase space factor corrected and background subtracted. Before the efficiency correction, we subtract the background with the shape on the distribution $m_{K^-\pi^+}$ versus $m_{K^+K^-}$ from MC. The distribution $m_{K^-\pi^+}$ versus $m_{K^+K^-}$ of MC is used to calculate the efficiency. Then we correct the

distributions with the efficiency and the phase space factor $1/\sqrt{1 - \frac{4m(K)^2}{m(K^+K^-)^2}}$, where $m(K)$ is the nominal mass of K^+ [12]. $Y_k^0(\cos\Theta)$ are normalized in the following formalism:

$$\int_{-1}^{1} Y_k^0(\cos\Theta)Y_j^0(\cos\Theta)d\cos\Theta = \frac{\delta_{kj}}{2\pi}, \qquad (3)$$

Considering the orthogonality condition, we can obtain the expansion coefficients according to Eq. 2 and Eq. 4:

$$\langle Y_k^0 \rangle = \int_{-1}^{1} Y_k^0(\cos\Theta)\frac{dN}{d\cos\Theta}d\cos\Theta. \qquad (4)$$

In this section, the formalism $\sum_{n=1}^{N} Y_k^0(\cos\Theta_n)$ is used to calculate the integral, where Θ_n refers to the Θ of the n-th event.

According to $\langle Y_k^0 \rangle = \sum_{n=1}^{N} Y_k^0(\cos\Theta_n)$, we can obtain the distribution of $\langle Y_k^0 \rangle$ for k = 0, 1 and 2 at the low end of K^+K^- mass spectrum $(0.988 < m(K^+K^-) < 1.15$ GeV/c^2), as shown in Fig. 3.

Assuming that only S- and P-wave amplitudes are necessary at the low end of K^+K^- mass spectrum, we can also write the distribution $\frac{dN}{d\cos\Theta}$ in terms of the partial wave amplitudes:

$$\frac{dN}{d\cos\Theta} = 2\pi \left| SY_0^0(\cos\Theta) + PY_1^0(\cos\Theta) \right|^2, \qquad (5)$$

where S and P refer to the amplitude of S-wave and P-wave, respectively. Comparing the coefficients of $Y_k^0(cos\Theta)$ in Eq. 2 and Eq. 5 [16], we can obtain

$$|S|^2 = \sqrt{4\pi}\langle Y_0^0 \rangle - \sqrt{5\pi}\langle Y_2^0 \rangle,$$
$$cos\phi_{SP} = \sqrt{\frac{\pi}{(\sqrt{4\pi}\langle Y_0^0 \rangle - \sqrt{5\pi}\langle Y_2^0 \rangle)\sqrt{5\pi}\langle Y_2^0 \rangle}}\langle Y_1^0 \rangle, \qquad (6)$$
$$|P|^2 = \sqrt{5\pi}\langle Y_2^0 \rangle,$$

where $\phi_{SP} = \phi_S - \phi_P$ is the phase different between S-wave and P-wave. Calculating $|S|^2$ (S(980)), ϕ_{SP} and $|P|^2$ in every mass interval of $m(K^+K^-$ in the threshold region, we can get the corresponding distributions, as shown in Fig. 4. There are two curves in Fig. 4(c) because of the sign ambiguity of ϕ_{SP} extracted from $cos\phi_{SP}$.

S(980) is empirically parameterized with the following formula:

$$A_{S(980)} = \frac{1}{m_0^2 - m^2 - im_0\Gamma_0\rho_{KK}}, \qquad (7)$$

where $\rho_{KK} = 2p/m$. Fitting the distribution of $|S|^2$ in Fig 4(a) with $|A_{S(980)}|^2$, we can obtain the values of m_0 and Γ_0:

$$m_0 = (0.919 \pm 0.006_{stat}) \text{ GeV}/c^2,$$
$$\Gamma_0 = (0.272 \pm 0.040_{stat}) \text{ GeV}. \qquad (8)$$

Fig. 5 shows the fit result with statistical errors only.

According to Eq. 8, the S(980) central mass is much lower than the threshold of $m(K^+K^-$ (about 0.988 GeV/c^2). So the distribution of ϕ_S is expected to be a flat curve decreasing slowly. Then the red curve decreasing rapidly near the nominal mass of $\phi(1020)$ is chosen as the physical solution. From Eq. 20 in Sec. V B 1, we can get the phase ϕ_P of $\phi(1020)$. Then we can obtain the phase of S(980) ϕ_S by adding ϕ_{SP} and ϕ_P, as shown in Fig 4(d). The values of $|S|^2$ (arbitrary units), $|P|^2$ (arbitrary units) and ϕ_S in every mass interval of the threshold region are listed in Table III.

Systematic uncertainties in this section taken in account:

- I Data-MC agreement for the BDTG output. We apply the same BDTG as that in this section to a control sample, which passed the same event selection without the kinematic fit χ_{5c}^2 cut criteria as that in Sec. V A, and compare the efficiency of data and MC. The efficiency of data (MC) is defined as $e_{data} = \frac{N_{d0}}{N_{d1}}$ ($e_{MC} = \frac{N_{M0}}{N_{M1}}$), where N_{d0} (N_{M0}) and N_{d1} (N_{M1}) are the number of events before and after applying the BDTG cut criteria. The comparison of efficiencies between data and MC is listed in Table IV. We fit the shape of S(980) corrected with $\frac{e_{data}}{e_{MC}}$ and take the shift of m_0 and Γ_0 as the systematic uncertainty. The shift of m_0 and Γ_0 are 0.03 GeV/c^2 and 0.02 GeV, respectively.

- II Background subtraction. We change the bin number and fit range and replace the background shape with a third-order Chebychev polynomial in the fit shown in Fig 2 and take the shift as a resource of background ratio error. We vary the background ratio ($(3.8 \pm 0.3)\%$) with one sigma and then take the largest shift of the fit of S(980) as the systematic uncertainty related to the background ratio. The background shape of generic MC is also replaced with that of "Sideband" $(1.90 < M(D_s) < 1.95$ GeV/c^2 and $1.986 < M(D_s) < 2.03$ GeV/c^2) for data to perform a fit and the shift is taken as the systematic uncertainty related to the background shape. The shift of m_0 and Γ_0 are 0.002 GeV/c^2 and 0.001 GeV.

- III Particle identification (PID) and tracking efficiency difference between data and MC. To estimate the experimental effects related to the difference of PID and tracking efficiency between data and MC, based on the work [18] and the work [19], we weight each event with the efficiency of data divided by that of MC and fit the shape of S(980). The shift of m_0 and Γ_0 are 0.001 GeV/c^2 and 0.013 GeV.

- IV The $f_0(1370)$ remained in S(980). We assume that the fit fraction (defined in Sec. V C) of $D_s^+ \to f_0(1370)\pi^+$ is 5% and then produced a MC sample with procedure $D_s^+ \to f_0(1370)\pi^+$

TABLE III. The values of $|S|^2$ (arbitrary units), $|P|^2$ (arbitrary units) and ϕ_S. The values of Uncertainties in the table are statistical only.

$m(K^+K^-)$ (GeV/c^2)	$|S|^2$ (arbitrary units)	$|P|^2$ (arbitrary units)	ϕ_S (degrees)
[0.988, 0.992]	14593 ± 1860	-1137 ± 1401	-
[0.992, 0.996]	11326 ± 1364	168 ± 1027	92 ± 48
[0.996, 1.000]	11064 ± 1143	-531 ± 850	-
[1.000, 1.004]	8659 ± 1015	1006 ± 748	90 ± 7
[1.004, 1.008]	7207 ± 1281	7292 ± 1003	80 ± 5
[1.008, 1.012]	8703 ± 1509	11746 ± 1200	81 ± 5
[1.012, 1.016]	6669 ± 2565	48763 ± 2066	79 ± 8
[1.016, 1.020]	7051 ± 6057	199740 ± 5048	101 ± 32
[1.020, 1.024]	2466 ± 4232	122645 ± 3520	96 ± 52
[1.024, 1.028]	4292 ± 2108	34363 ± 1748	87 ± 14
[1.028, 1.033]	4009 ± 1455	15046 ± 1212	81 ± 13
[1.033, 1.037]	3922 ± 1088	8108 ± 887	78 ± 14
[1.037, 1.041]	3480 ± 944	5945 ± 768	70 ± 14
[1.041, 1.045]	5376 ± 854	3707 ± 678	71 ± 14
[1.045, 1.049]	4043 ± 696	2103 ± 551	76 ± 14
[1.049, 1.053]	3621 ± 665	1858 ± 530	76 ± 14
[1.053, 1.057]	3167 ± 599	1680 ± 467	76 ± 14
[1.057, 1.061]	3063 ± 569	1333 ± 448	70 ± 15
[1.061, 1.065]	3841 ± 582	685 ± 461	59 ± 17
[1.065, 1.069]	3343 ± 439	-45 ± 324	-
[1.069, 1.073]	3377 ± 525	395 ± 413	59 ± 21
[1.073, 1.077]	2635 ± 474	684 ± 368	71 ± 15
[1.077, 1.081]	2632 ± 426	357 ± 320	64 ± 18
[1.081, 1.085]	2802 ± 485	647 ± 377	63 ± 16
[1.085, 1.089]	2121 ± 421	287 ± 332	74 ± 18
[1.089, 1.093]	2487 ± 369	-185 ± 278	-
[1.093, 1.097]	2105 ± 505	1041 ± 409	68 ± 15
[1.097, 1.101]	2326 ± 440	100 ± 355	51 ± 66
[1.101, 1.105]	1962 ± 369	47 ± 286	44 ± 137
[1.105, 1.109]	1422 ± 323	216 ± 246	65 ± 21
[1.109, 1.114]	1420 ± 453	777 ± 377	63 ± 17
[1.114, 1.118]	697 ± 377	903 ± 307	73 ± 17
[1.118, 1.122]	1351 ± 330	234 ± 257	65 ± 21
[1.122, 1.126]	1373 ± 297	-60 ± 229	-
[1.126, 1.130]	690 ± 312	340 ± 255	59 ± 22
[1.130, 1.134]	535 ± 246	130 ± 197	67 ± 27
[1.134, 1.138]	772 ± 261	205 ± 199	38 ± 37
[1.138, 1.142]	1246 ± 266	-71 ± 200	-
[1.142, 1.146]	545 ± 350	456 ± 298	35 ± 37
[1.146, 1.150]	763 ± 262	206 ± 205	58 ± 24

TABLE IV. The comparison of efficiencies between data and MC.

| $m_{K^+K^-}$ (GeV/c^2)	e_{data}	e_{MC}	e_{data}/e_{MC}
[0.988, 1.014]	0.3134 ± 0.0273	0.3069 ± 0.0062	1.0210 ± 0.0914
[1.014, 1.018]	0.3199 ± 0.0278	0.3641 ± 0.0068	0.8787 ± 0.0781
[1.018, 1.019]	0.3968 ± 0.0357	0.4059 ± 0.0080	0.9775 ± 0.0900
[1.019, 1.021]	0.3631 ± 0.0320	0.3970 ± 0.0083	0.9146 ± 0.0830
[1.021, 1.023]	0.3704 ± 0.0330	0.3834 ± 0.0075	0.9662 ± 0.0881
[1.023, 1.029]	0.3028 ± 0.0261	0.3190 ± 0.0064	0.9491 ± 0.0840
[1.029, 1.061]	0.2932 ± 0.0254	0.2962 ± 0.0059	0.9900 ± 0.0878
[1.061, 1.150]	0.2440 ± 0.0201	0.2502 ± 0.0049	0.9750 ± 0.0829
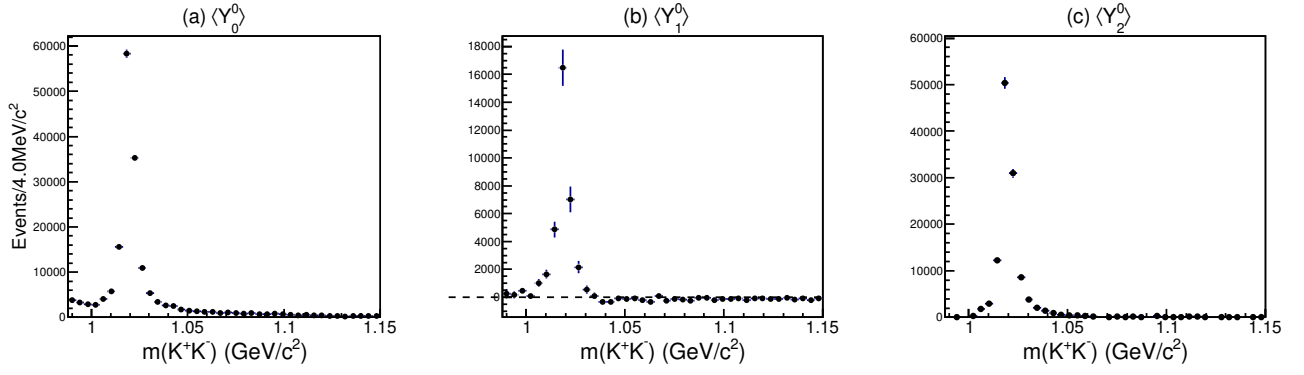
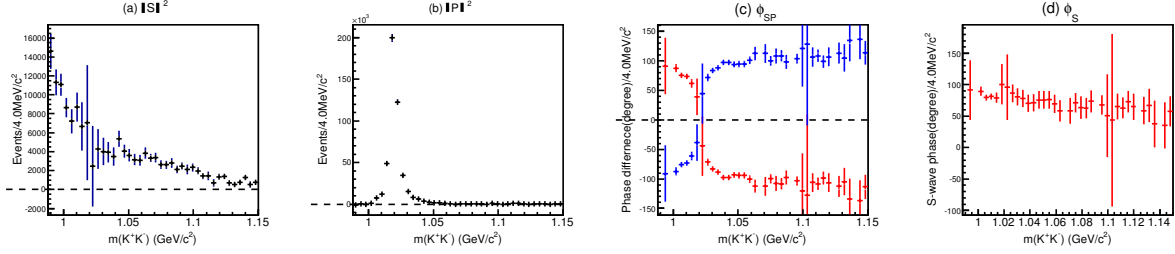FIG. 3. The distribution of $\langle Y_k^0 \rangle$ for k = 0, 1 and 2 in K^+K^- threshold region.

FIG. 4. The distribution of $|S|^2$ (a), $|P|^2$ (b), ϕ_{SP} and ϕ_S in the threshold region of $m(K^+K^-)$.

$\Gamma_0 = 0.272 \pm 0.040$ GeV
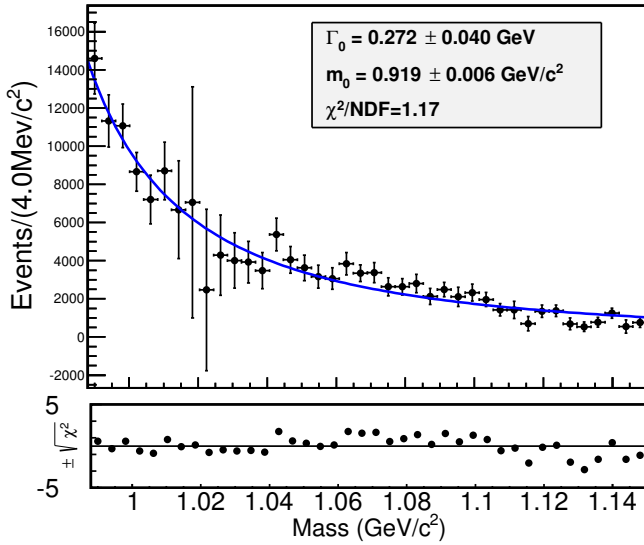
$m_0 = 0.919 \pm 0.006$ GeV/c²

χ^2/NDF=1.17

FIG. 5. Fit of S(980) amplitudes with $|A_{S(980)}|^2$.

(a) $|S|^2$
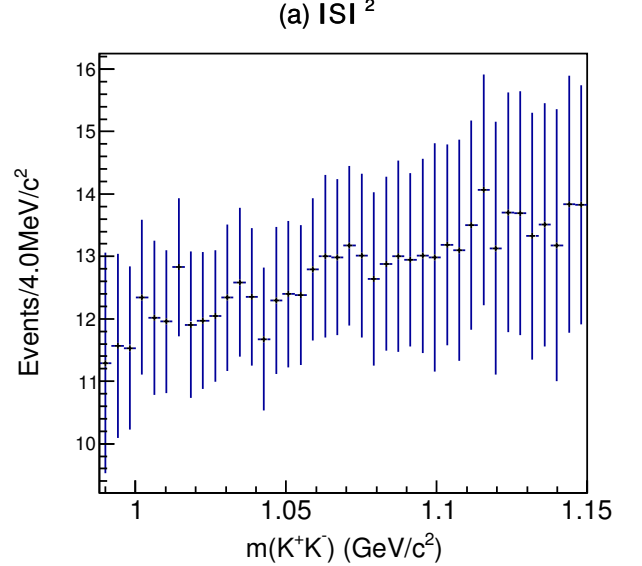
FIG. 6. The shape of $f_0(1370)$ at the low end of $m_{K^+K^-}$ mass spectrum extracted from a MC sample with procedure $D_s^+ \to f_0(1370)\pi^+$.

to extract the shape of $f_0(1370)$ at the low end of $m_{K^+K^-}$ mass spectrum. We scale the number of $D_s^+ \to f_0(1370)\pi^+$ according to the fit fraction of $D_s^+ \to f_0(1370)\pi^+$ and the shape contributed from $f_0(1370)$ is shown in Fig. 6. At last, the $f_0(1370)$ remained in S(980) is subtracted according to the scaled shape obtained above. The shift of m_0 and Γ_0 are 0.001 GeV/c² and 0.003 GeV.

- V Fit range. We vary the fit range from [0.988, 1.15] GeV/c² to [0.988, 1.145] GeV/c² and the shift of m_0 and Γ_0 are 0.002 GeV/c² and 0.003 GeV.

All of the systematic uncertainties mentioned above are summarized in Table V. We obtain the result of m_0

TABLE V. Systematic uncertainties of partial wave analysis in the low K^+K^- mass region.

Source	m_0 (GeV/c^2)	Γ_0 (GeV)
BDTG	0.030	0.020
Background subtraction	0.002	0.001
PID and Tracking	0.001	0.013
$f_0(1370)$	0.001	0.003
Fit range	0.002	0.003
total	0.030	0.024

and Γ_0 with statistical and systematic errors to be:

$$m_0 = (0.919 \pm 0.006_{stat} \pm 0.030_{sys}) \text{ GeV}/c^2,$$
$$\Gamma_0 = (0.272 \pm 0.040_{stat} \pm 0.024_{sys}) \text{ GeV}, \qquad (9)$$

V. AMPLITUDE ANALYSIS

An unbinned maximum likelihood method is used to determine the intermediate resonance composition in the decay $D_s \to K^+K^-\pi^+$. The likelihood function is constructed with the probability density function (PDF), in which the momenta of the three daughter particles are used as inputs.

A. double tag method in amplitude analysis

As D_s mesons should be produced in pairs, D_s mesons can be reconstructed with double tag (DT) method. In the single tag (ST) sample, only one D_s^+ or D_s^- meson is reconstructed through chosen D_s decays, which are so called tag modes. Eight tag modes used in the amplitude analysis and Sec. VI are $D_s^- \to K^+K^-\pi^-$, $D_s^- \to K_S^0 K^-$, $D_s^- \to K_S^0 K^-\pi^+\pi^-$, $D_s^- \to K^-\pi^+\pi^-$, $D_s^- \to K_S^0 K^+\pi^-\pi^-$, $D_s^- \to \pi^+\pi^-\pi^-$, $D_s^- \to \eta'_{\pi^+\pi^-\eta_{\gamma\gamma}}$, $D_s^- \to K^+K^-\pi^-\pi^0$. However, in the DT sample, both tagged D_s^- and signal D_s^+ are reconstructed. After $K^\pm$, K_S^0, η, η' and π^0 are identified in Sec. III, with the tagged D_s^- meson, the signal D_s^+ can be reconstructed with the DT method. A five-constraint (5C) kinematic fit, in which four-momentum of $D_s D_s^*$ is constrained to the initial four-momentum and the invariant mass of D_s^* is constrained to the corresponding PDG values [12], is performed to ensure that all events fall within Dalitz plot. If the combination of signal D_s and extra γ, which is used to reconstruct neither signal D_s^+ nor D_s^-, to form D_s^* have a lower χ^2_{5C} than that of tagged D_s and γ, the signal D_s should come from the D_s^* decay. Otherwise, the signal D_s should directly come from the intersection point. If there are duplicate candidates of $D_s^* D_s$ pairs in an event, the candidate with minimum χ^2_{5C} is selected as the best candidate. The candidates satisfy

- m_{sig} and m_{tag} falls in the mass regions shown in Table VI,

- $\chi^2_{5C} < 200$,

are retained for the amplitude analysis, where m_{sig} and m_{tag} refer to mass of D_s at signal side and tag side respectively.

TABLE VI. The mass windows for each tag mode. The mass windows use the results in Ref. [17]

Tag mode	Mass window (GeV/c^2)
$D_s^- \to K_S^0 K^-$	[1.948, 1.991]
$D_s^- \to K^+K^-\pi^-$	[1.950, 1.986]
$D_s^- \to K^+K^-\pi^-\pi^0$	[1.947, 1.982]
$D_s^- \to K_S^0 K^-\pi^+\pi^-$	[1.958, 1.980]
$D_s^- \to K_S^0 K^+\pi^-\pi^-$	[1.953, 1.983]
$D_s^- \to \pi^-\pi^-\pi^+$	[1.952, 1.984]
$D_s^- \to \pi^-\eta'_{\pi^+\pi^-\eta_{\gamma\gamma}}$	[1.940, 1.996]
$D_s^- \to K^-\pi^+\pi^-$	[1.953, 1.983]

In addition, we use the four-momentum after applying kinematic fitting with the mass of signal D_s constrained to PDG value and the five constrains above to perform amplitude analysis.

The background of the DT sample in the amplitude analysis is estimated with the generic MC. There is no obvious peaking background in the signal region (1.950 $< m_{sig} <$1.986 GeV/c^2) and 4381 signal candidates with a purity of 99.6% are obtained with all selection criteria applied.

B. Likelihood Function Construction

As this decay is a three-body process, the amplitude $A_n(p)$ for the nth amplitude mode is given by

$$A_n(p) = P_n(p)S_n(p)F_n^r(p)F_n^D(p), \qquad (10)$$

where p refers to the set of the three daughter particles' four-momenta, $P_n(p)$ is the propagator, $S_n(p)$ is the spin factor constructed with the covariant tensor formalism [20], $F_n^r(p)$ and $F_n^D(p)$ are the Blatt-Weisskopf barrier factor for the intermediate resonance and D_s meson, respectively. According to the isobar formulation, the total amplitude $M(p)$ is obtained by the coherent sum of all intermediate modes:

$$M(p) = \sum c_n A_n(p), \qquad (11)$$

where $c_n = \rho_n e^{i\phi}$ is the complex coefficient of the nth mode, ρ_n and ϕ_n are the magnitude and phase of c_n,

respectively. Then The signal PDF $f_S(p)$ is presented as:

$$f_S(p) = \frac{\epsilon(p)\,|M(p)|^2\,R_3(p)}{\int \epsilon(p)\,|M(p)|^2\,R_3(p)\,dp}, \qquad (12)$$

where $\epsilon(p)$ is the detection efficiency and $R_s(p)$ indicates the three-particle phase space, which is defined as:

$$R_3(p)dp = (2\pi)^4\delta^4\left(p_{D_s} - \sum_{\alpha=1}^{3} p_\alpha\right) \prod_{\alpha=1}^{3} \frac{d^3 p_\alpha}{(2\pi)^3 2E_\alpha}, \quad (13)$$

where $\alpha = 1, 2, 3$ is the index of the three daughter particles. Considering the background ratio is only 0.4%, the likelihood function is given by

$$\begin{aligned}
\ln \mathcal{L} &= \sum_{k}^{N_{data}} \ln f_S(p^k) \\
&= \sum_{k}^{N_{data}} \ln \left(\frac{|M(p)|^2}{\int \epsilon(p)\,|M(p)|^2\,R_3(p)\,dp} \right), \qquad (14) \\
&+ \sum_{k}^{N_{data}} \ln \left(R_3(p)\epsilon(p) \right)
\end{aligned}$$

where N_{data} is the number of candidate events in data. The normalization integral in Eq. 14 is firstly determined by the following equation using a phase-space MC sample with a uniform distribution:

$$\begin{aligned}
&\int \epsilon(p)\,|M(p)|^2\,R_3(p)\,dp \\
&\approx \frac{1}{N_{MC,gen}} \sum_{k_{MC}}^{N_{MC,sel}} \left| M(p^{k_{MC}}) \right|^2,
\end{aligned} \qquad (15)$$

where $p^{k_{MC}}$ is the k_{MC}^{th} MC event's set of four-momenta. Here, $N_{MC,gen}$ and $N_{MC,sel}$ are the numbers of generated phase-space events and selected phase-space events, respectively. A set of estimated c_n can be obtained using the phase-space MC to perform the normalization integral. Assuming the estimated values to be c'_n, we can perform the normalization integral with signal MC samples:

$$\begin{aligned}
&\int \epsilon(p)\,|M(p)|^2\,R_3(p)\,dp \\
&\approx \frac{1}{N_{MC}} \sum_{k_{MC}}^{N_{MC}} \frac{\left| M(p^{k_{MC}}) \right|^2}{\left| M^{gen}(p^{k_{MC}}) \right|^2},
\end{aligned} \qquad (16)$$

where $M^{gen}(p^{k_{MC}})$ is the PDF modeled with c'_n to generate signal MC and N_{MC} is the number of the signal MC sample. γ_ϵ is introduced to correct the bias caused by PID and tracking efficiency inconsistencies between data and MC:

$$\gamma_\epsilon = \prod_j \frac{\epsilon_{j,data}(p)}{\epsilon_{j,MC}(p)}, \qquad (17)$$

where $\epsilon_{j,data}$ and $\epsilon_{j,MC}$ refer to the PID or tracking efficiencies modeled with p for data and MC, respectively.

Taking the correction factors γ_ϵ in account, then the normalization integral can be obtained by:

$$\begin{aligned}
&\int \epsilon(p)\,|M(p)|^2\,R_3(p)\,dp \\
&\approx \frac{1}{N_{MC}} \sum_{k_{MC}}^{N_{MC}} \frac{\left| M(p^{k_{MC}}) \right|^2 \gamma_\epsilon}{\left| M^{gen}(p^{k_{MC}}) \right|^2}.
\end{aligned} \qquad (18)$$

1. Propagator and Blatt-Weisskopf barrier

For a given two-body decay $a \to bc$, p_a, p_b and p_c are denoted to the momenta of particles a, b and c. s_a, s_b and s_c refer to the squared invariant mass of particles a, b and c. $r_a = p_a - p_c$ is the momentum difference between a and b. q is defined as the magnitude of the momentum of b or c in the rest system of a:

$$q = \sqrt{\frac{(s_a + s_b + s_c)^2}{4s_a} - s_b}. \qquad (19)$$

The intermediate resonances $K^*(892)^0$, $f_0(1710)$, $f_0(1370)$ and $\phi(1020)$ are parameterized as a relativistic Breit-Wigner (RBW) formula,

$$\begin{aligned}
P &= \frac{1}{(m_0^2 - s_a) - im_0\Gamma(m)}, \\
\Gamma(m) &= \Gamma_0 \left(\frac{q}{q_0}\right)^{2L+1} \left(\frac{m_0}{m}\right) \left(\frac{X_L(q)}{X_L(q_0)}\right)^2,
\end{aligned} \qquad (20)$$

where m_0 and Γ_0 are the mass and the width of the intermediate resonances, and are fixed to the PDG values [12] except the mass and the width of $f_0(1370)$. The mass and width of $f_0(1370)$ are fixed to 1350 MeV/c^2 and 265 MeV/c^2 [21], respectively.. The value of q_0 in Eq. 20 is that of q when $s_a = m_0^2$, L denotes the angular momenta and $X_L(q)$ is defined as:

$$\begin{aligned}
X_{L=0}(q) &= 1, \\
X_{L=1}(q) &= \sqrt{\frac{2}{z^2+1}}, \\
X_{L=2}(q) &= \sqrt{\frac{13}{9z^4+3z^2+1}},
\end{aligned} \qquad (21)$$

where $z = qR$. Only the intermediate resonances with angular momenta less than three are retained as the limit of phase space. The R is the effective radius of the intermediate resonance or D_s meson. The values of R are fixed to 3.0 GeV^{-1} for intermediate states and 5.0 GeV^{-1} for D_s meson [22], respectively. The values of R will be varied to obtain the corresponding systematic uncertainty.

$K_0^*(1430)^0$ is parameterized with Flatte formula:

$$P_{K_0^*(1430)^0} = \frac{1}{M^2 - s - i(g_1\rho_{K\pi}(s) + g_2\rho_{\eta'K}(s))}, \quad (22)$$

where s is the squared $K^-\pi^+$ invariant mass, $\rho_{K\pi}(s)$ and $\rho_{\eta'K}(s)$ are Lorentz invariant PHSP factor, and $g_{1,2}$ are

coupling constants to the corresponding final state. The parameters of $K_0^*(1430)^0$ are fixed to values measured by CLEO [23].

For resonance S(980) ($f_0(980)$ and $a_0(980)$), we use Eq. 7 to describe the propagator and the values of parameters are fixed to the values in Eq. 8 obtained from the model independent partial wave analysis section (Sec. V).

The Blatt-Weisskopf barriers are given by

$$F_L(q) = z^L X_L(q). \tag{23}$$

2. Spin Factors

The spin projection operators [20] for a two-body decay are defined as

$$
\begin{aligned}
P^0(a) &= 1, \\
P^{(1)}_{\mu\mu'}(a) &= -g_{\mu\mu'} + \frac{p_{a,\mu}p_{a,\mu'}}{p_a^2}, \\
P^{(2)}_{\mu\nu\mu'\nu'}(a) &= \frac{1}{2}(P^{(1)}_{\mu\mu'}(a)P^{(1)}_{\nu\nu'}(a) + P^{(1)}_{\mu\nu'}(a)P^{(1)}_{\nu\mu'}(a)) \\
&\quad + \frac{1}{3}P^{(1)}_{\mu\nu}(a)P^{(1)}_{\mu'\nu'}(a).
\end{aligned}
\tag{24}
$$

The corresponding covariant tensors are written in the following formalism

$$
\begin{aligned}
\tilde{t}^{(0)}(a) &= 1, \\
\tilde{t}^{(1)}_\mu(a) &= -P^{(1)}_{\mu\mu'}(a)r_a^{\mu'}, \\
\tilde{t}^{(2)}_{\mu\nu}(a) &= P^{(2)}_{\mu\nu\mu'\nu'}(a)r_a^{\mu'}r_a^{\nu'}.
\end{aligned}
\tag{25}
$$

The spin factor for the process $D_s \to aX$ (X refers to the daughter particle directly decayed from D_s meson) with $a \to bc$ is,

$$
\begin{aligned}
S_n &= 1, \\
S_n &= \tilde{T}^{(1)\mu}(D_s)\tilde{t}^{(1)}_\mu(a), \\
S_n &= \tilde{T}^{(2)\mu\nu}(D_s)\tilde{t}^{(2)}_{\mu\nu}(a),
\end{aligned}
\tag{26}
$$

where $\tilde{T}^{(L)}_\mu(D_s)$ and $\tilde{t}^{(L)}_\mu(a)$ are the covariant tensors with angular momenta L for $D_s \to aX$ and $a \to bc$, respectively.

C. Fit Fraction

With the fit result of c_n, the fit fraction (FF) is calculated with a phase-space MC at the generator level

$$FF(n) = \frac{\sum_{k=1}^{N_{MC,gen}} |c_n A_n|^2}{\sum_{k=1}^{N_{MC,gen}} |M(p_j^k)|^2}, \tag{27}$$

where $N_{MC,gen} = 2000000$, is the number of the PHSP MC events at generator level.

We randomly vary the coefficients c_n according to the corresponding error matrix and then we can obtain a series of FFs for each intermediate process. A Gaussian function is used to fit the distribution for each intermediate process and we take the width of the Gaussian function as the corresponding statistical uncertainty of FF. In this analysis, the coefficients are varied 2000 times to obtain the statistical uncertainties of FFs.

D. Fit Result

Figure 7 shows the Dalitz plot of $m^2(K^+K^-)$ versus $m^2(K^-\pi^+)$. A clear peak of $K^*(892)^0$ and $\phi(1020)$ can be seen in the plot. We choose $K^*(892)^0$ as the reference and the magnitude ρ_n and phase ϕ_n for $D_s^+ \to K^*(892)^0K^+$ are fixed to 1.0 and 0.0, respectively. The magnitude and phase of other processes are floated in the fit. Other possible processes are added one by one into the fit according to their statistical significances. We calculate the statistical significance for a certain intermediate process using the likelihood shift $\Delta \ln \mathcal{L}$ with or without the process. Only the processes each with a statistical significance less than 5σ are discarded. The six intermediate processes retained in the nominal fit are $D_s^+ \to \bar{K}^*(892)^0K^+$, $D_s^+ \to \phi(1020)\pi^+$, $D_s^+ \to S(980)\pi^+$, $D_s^+ \to \bar{K}_0^*(1430)^0K^+$, $D_s^+ \to f_0(1370)\pi^+$ and $D_s^+ \to f_0(1710)\pi^+$.
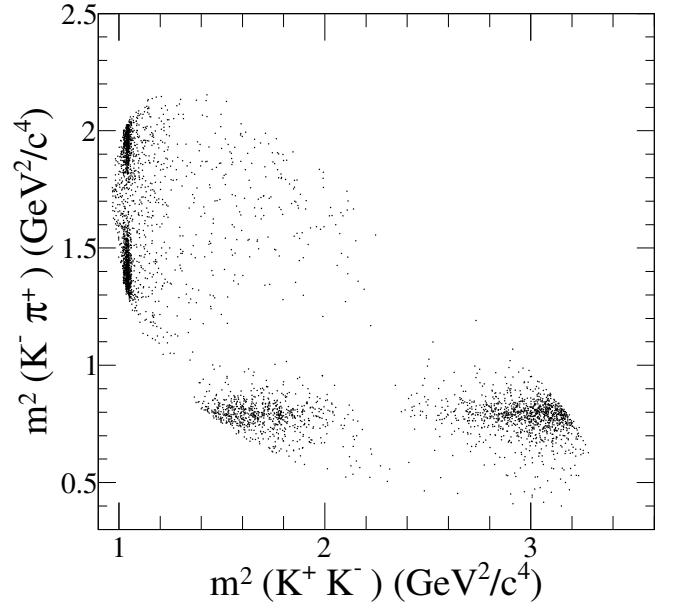

FIG. 7. The Dalitz plot of $m^2(K^-\pi^+)$ versus $m^2(K^+K^-)$ after event selection.

Signal MC samples modeled with the fit result of the nominal fit, called AA signal MC samples, are generated to compare the projections of the Dalitz plots and calculate the fit bias, which will be discussed in Sec. V E. The

Dalitz plot projections are shown in Fig. 8. Calculating the χ_2 of the fit using an adaptive binning of the Dalitz plot, in which each bin has at 10 events, of $m^2(K^+K^-)$ versus $m^2(K^-\pi^+)$ gives the goodness of fit, the value of which is $\chi^2/NDOF = 290.0/280$

We also compare the shape of S wave extracted from data in Fig. 4 (Sec. IV) and the projection of S wave ($S(980)$, $\bar{K}_0^*(1430)^0$, $f_0(1710)$ and $f_0(1370)$) to $m(K^+K^-)$ in the nominal fit, shown in Fig. 9. We can see that the two shapes are well consistent and the other wave components' (except S(980)) contribution is very small.

E. Systematic Uncertainty

The following categories of systematic uncertainties for the amplitude analysis are studied:

- I Propagator parameterizations of the resonances. The masses and widths of resonances are varied within one σ error.

  – For $S(980)$, m_0 and Γ_0 are shifted within errors from Eq. 9 in Sec. IV.

  – For $f_0(1370)$, the mass and width are shifted within errors from Ref. [21].

  – For $\bar{K}_0^*(1430)^0$, the parameters are shifted within errors from Ref. [23].

  – For other states, uncertainties are taken from PDG [12].

- II The systematic uncertainties related to the effective radius of Blatt-Weisskopf Barrier (R). The effective radius of Blatt-Weisskopf Barrier is varied within the range $[1.0, 5.0]$ GeV^{-1} for intermediate resonances and $[3.0, 7.0]$ GeV^{-1} for D_s mesons.

- III Fit bias. Pull distribution checks using 300 AA signal MC samples are performed to obtain the fit bias. Here the pull value PULL for a certain parameter x is defined as $\text{PULL} = (x_{data} - x_{MC})/\sigma_{x_{MC}}$, where x_{MC} and $\sigma_{x_{MC}}$ are the value and the statical error of x obtained from the fit to a certain AA signal MC sample and x_{data} refers to the value of x in the nominal fit. The AA signal MC samples are generated each with the same size of the data. A Gaussian function is used to fit each pull distribution. The quadrature sum of the mean value and the error of mean in the pull distribution fit is taken as the corresponding systematic uncertainty in unit of the corresponding statistical error.

- IV Experimental effects. The experimental effects are related to the acceptance difference between MC and data caused by PID and tracking efficiencies, that is γ_ϵ in Eq. 17. The uncertainties caused by γ_ϵ is obtained by performing alternative amplitude analyses varying PID and tracking efficiencies according to their uncertainties according to the work [18] and the work [19].

- V Model assumptions. We replace Eq. 22 with LASS model [27]. And then take the shift of parameters as the uncertainties.

All of the systematic uncertainties of the magnitudes, phases and FFs are listed in Table VII.

VI. BRANCHING FRACTION

A. Efficiency and Data Yields

After the selection described in Sec. III, DT method is also used to perform the branching fraction measurement. We use the same eight tag modes as that in Sec. V. For each tag mode, if there are duplicate tag D_s candidates in an event, only the candidate with M_{rec} closest to the nominal mass of D_s^* [12] is retained. Then the ST yields can be obtained by the fits to the D_s invariant mass distributions, as shown in Fig. 10. In the fit, the mass windows of the tag modes are set to be the same as the Ref. [17]. The signal shape is modeled as MC shape convoluted with a Gaussian function, while background is parameterized as the second-order Chebychev polynomial. The fits to generic MC are performed to estimate the corresponding ST efficiencies. The ST yields (Y_{ST}) and ST efficiencies (ϵ_{ST}) are listed in Table IX.

After the best candidates of ST D_s^- mesons is identified, we search for the $D_s^+ \to K^+K^-\pi^+$. Only one DT D_s^+ candidate, if exists, with the minimum average mass (aM) of tag D_s and signal D_s^+ is retained for each tag mode in an event. The DT efficiencies, listed in Table X are obtained based on the AA signal MC.

As $D_s^- \to K^+K^-\pi^-$ is not only our signal mode but also one of our tag modes, we divide the events into two categories:

- Cat. A: Tag D_s decays to tag modes except $D_s^- \to K^+K^-\pi^-$. The generic MC sample with the signal removed shows no peaking background around the fit range of $1.90 < M_{sig} < 2.03$ GeV/c^2. Thus, the double tag yield is determined by the fit to M_{sig}, shown in Fig. 11(a). The background is described with second-order Chebychev polynomial. The double tag yield is 3497 ± 64.

- Cat. B: Tag D_s decays to $K^+K^-\pi^+$. As both of the two D_s mesons decay to our signal modes, we fit dM (the mass of D_s at signal side minus that of tag side), which is shown in Fig. 11(b). Here, the background is described by a second-order Chebychev polynomial. The double tag yield is 1651 ± 42.
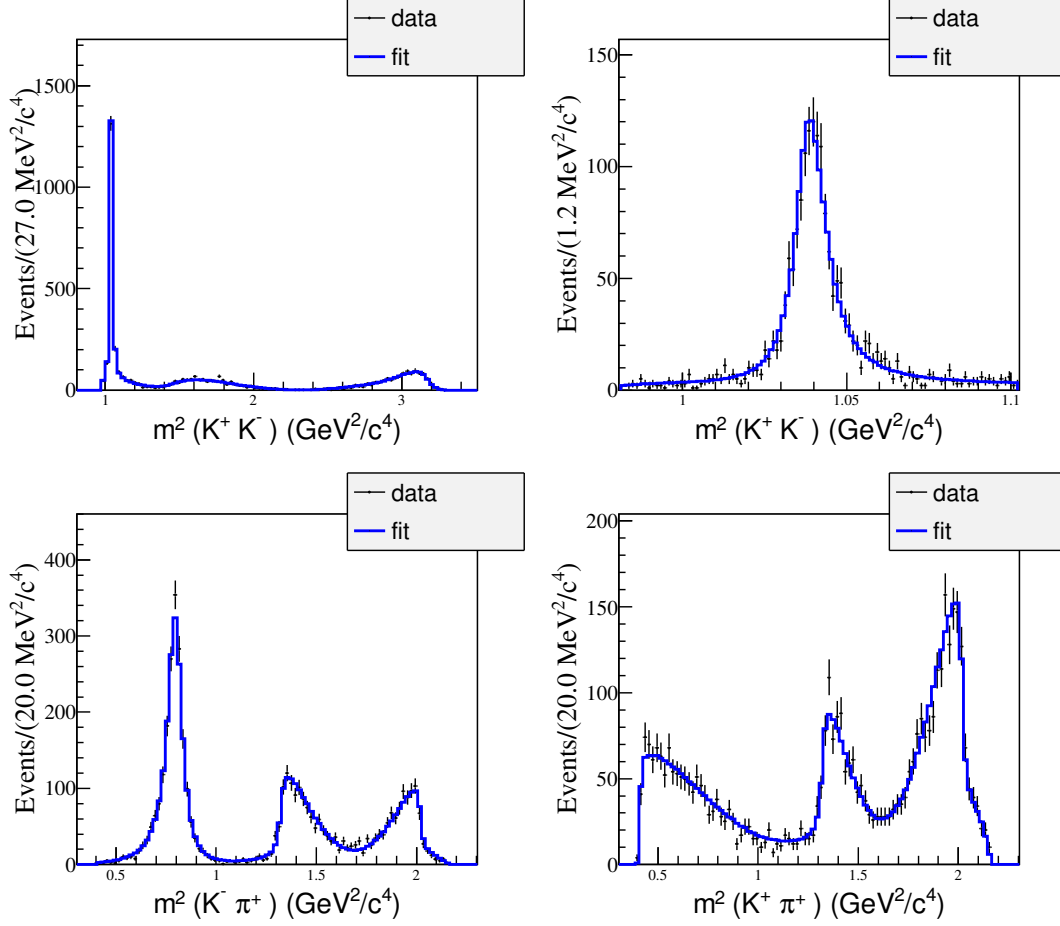
FIG. 8. $D_s^+ \to K^+ K^- \pi^+$: Dalitz plot projections from the nominal fit. The data are represented by points with error bars and the solid lines indicate the AA signal MC sample.

TABLE VII. Systematic uncertainties on the ϕ and FFs for different amplitudes in units of the corresponding statistical uncertainties.

Amplitude		Source					
		I	II	III	IV	V	Total
$D_s^+ \to \bar{K}^*(892)^0 K^+$	FF	0.32	0.29	0.14	0.41	0.12	0.62
$D_s^+ \to \phi(1020)\pi^+$	ϕ	0.49	0.10	0.06	0.07	0.05	0.51
	ρ	0.49	0.14	0.08	0.41	0.15	0.68
	FF	0.44	1.13	0.04	0.40	0.06	1.28
$D_s^+ \to S(980)\pi^+$	ϕ	0.98	0.25	0.04	0.11	0.04	1.02
	ρ	1.11	0.17	0.09	0.11	0.20	1.15
	FF	1.16	0.15	0.04	0.09	0.05	1.18
$D_s^+ \to \bar{K}_0^*(1430)^0 K^+$	ϕ	1.02	0.48	0.05	0.21	0.07	1.15
	ρ	1.00	0.36	0.15	0.20	0.14	1.10
	FF	0.76	0.35	0.11	0.22	0.11	0.88
$D_s^+ \to f_0(1710)\pi^+$	ϕ	0.31	0.25	0.04	0.14	0.13	0.45
	ρ	1.17	1.23	0.09	0.11	0.09	1.70
	FF	0.71	1.21	0.04	0.16	0.04	1.42
$D_s^+ \to f_0(1370)\pi^+$	ϕ	2.66	0.27	0.12	0.09	0.21	2.68
	ρ	1.01	0.32	0.21	0.09	0.04	1.06
	FF	0.42	0.30	0.15	0.06	0.13	0.56

TABLE VIII. The final results of the magnitudes, phases and fit fractions for the six amplitudes. The first and second uncertainties are the statistical and systematic uncertainties, respectively.

Amplitude	Magnitude	Phase	Fit fractions (%)	Significance (σ)
$D_s^+ \to \bar{K}^*(892)^0 K^+$	1.0 (fixed)	0.0 (fixed)	48.3±0.9±0.6	> 20
$D_s^+ \to \phi(1020)\pi^+$	1.09±0.02±0.01	6.22±0.07±0.04	40.5±0.7±0.9	> 20
$D_s^+ \to S(980)\pi^+$	2.88±0.14±0.16	4.77±0.07±0.07	19.3±1.7±2.0	> 20
$D_s^+ \to \bar{K}_0^*(1430)^0 K^+$	1.26±0.14±0.15	2.91±0.20±0.23	3.0±0.6±0.5	8.6
$D_s^+ \to f_0(1710)\pi^+$	0.79±0.08±0.14	1.02±0.12±0.05	1.9±0.4±0.6	9.2
$D_s^+ \to f_0(1370)\pi^+$	0.58±0.08±0.08	0.59±0.17±0.46	1.2±0.4±0.2	6.4

TABLE IX. The ST yields (Y_{ST}) and ST efficiencies (ϵ_{ST}). The mass windows use the results in Ref. [17]. The BFs of the sub-particle (K_S^0, π^0, η and $\eta^{'}$) decays are not included.

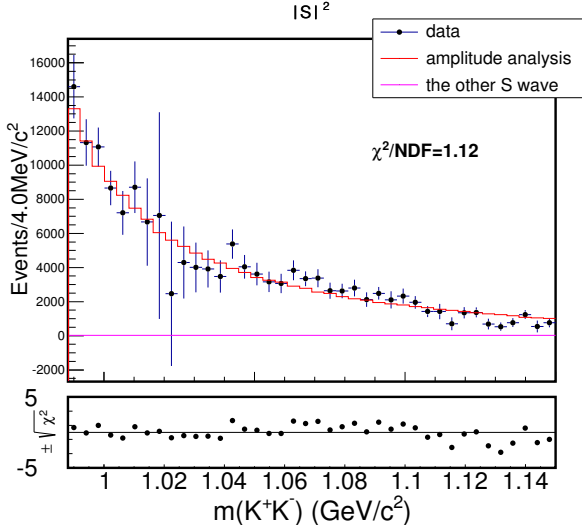| Tag mode	Mass window (GeV/c^2)	Y_{ST}	$\epsilon_{ST}(\%)$
$D_s^- \to K_S^0 K^-$	[1.948, 1.991]	31987 ± 314	49.09 ± 0.07
$D_s^- \to K^+ K^- \pi^-$	-	141189 ± 643	42.17 ± 0.03
$D_s^- \to K^+ K^- \pi^0_{\gamma\gamma}$	[1.947, 1.982]	37899 ± 1739	10.61 ± 0.03
$D_s^- \to K_S^0 K^- \pi^+ \pi^-$	[1.958, 1.980]	7999 ± 236	19.30 ± 0.12
$D_s^- \to K_S^0 K^+ \pi^- \pi^-$	[1.953, 1.983]	15723 ± 290	22.72 ± 0.06
$D_s^- \to \pi^- \pi^- \pi^+$	[1.952, 1.984]	38157 ± 873	56.94 ± 0.17
$D_s^- \to \pi^- \eta^{'}_{\pi^+\pi^-\eta_{\gamma\gamma}}$	[1.940, 1.996]	8009 ± 142	20.43 ± 0.06
$D_s^- \to K^- \pi^+ \pi^-$	[1.953, 1.983]	17112 ± 561	47.18 ± 0.22

FIG. 9. The comparison of S wave extracted from data in Fig. 4 (Sec. IV) and the projection of S wave (S(980), $\bar{K}_0^*(1430)^0$, $f_0(1710)$ and $f_0(1370)$) to $m(K^+K^-)$ in the nominal fit. The black dots with error bars refer to data, the purple line refers to the projection of the other S wave components except S(980) and the red line refers to the projection of S wave.

TABLE X. The DT efficiencies (ϵ_{DT}).The BFs of the sub-particle (K_S^0, π^0, η and $\eta^{'}$) decays are not included.

Tag mode	$\epsilon_{DT}(\%)$
$D_s^- \to K_S^0 K^-$	19.77±0.14
$D_s^- \to K^+ K^- \pi^-$	17.41±0.06
$D_s^- \to K^+ K^- \pi^0$	4.69±0.03
$D_s^- \to K_S^0 K^- \pi^+ \pi^-$	8.04±0.11
$D_s^- \to K_S^0 K^+ \pi^- \pi^-$	9.35±0.09
$D_s^- \to \pi^- \pi^- \pi^+$	23.72±0.15
$D_s^- \to \pi^- \eta^{'}_{\pi^+\pi^-\eta_{\gamma\gamma}}$	8.70±0.11
$D_s^- \to K^- \pi^+ \pi^-$	19.68±0.13

B. Tagging Technique and Branching Fraction

For the DT sample with only one tag mode, we have

$$Y_{ST} = 2N_{D_s^+ D_s^-} \mathcal{B}_{tag} \epsilon_{tag}, \quad (28)$$

$$\begin{aligned} N_{sig}^{obsA} &= 2N_{D_s^+ D_s^-} \mathcal{B}_{tag} \mathcal{B}_{sig} \epsilon_{tag,sig}, \quad \text{for Cat. A} \\ N_{sig}^{obsB} &= N_{D_s^+ D_s^-} \mathcal{B}_{tag} \mathcal{B}_{sig} \epsilon_{tag,sig}, \quad \text{for Cat. B} \end{aligned} \quad (29)$$

where $N_{D_s^+ D_s^-}$ is the total number of $D_s^{*\pm} D_s^{\mp}$ produced from $e^+ e^-$ collision; Y_{ST} is the number of observed tag modes; N_{sig}^{obsA} and N_{sig}^{obsB} are the number of observed
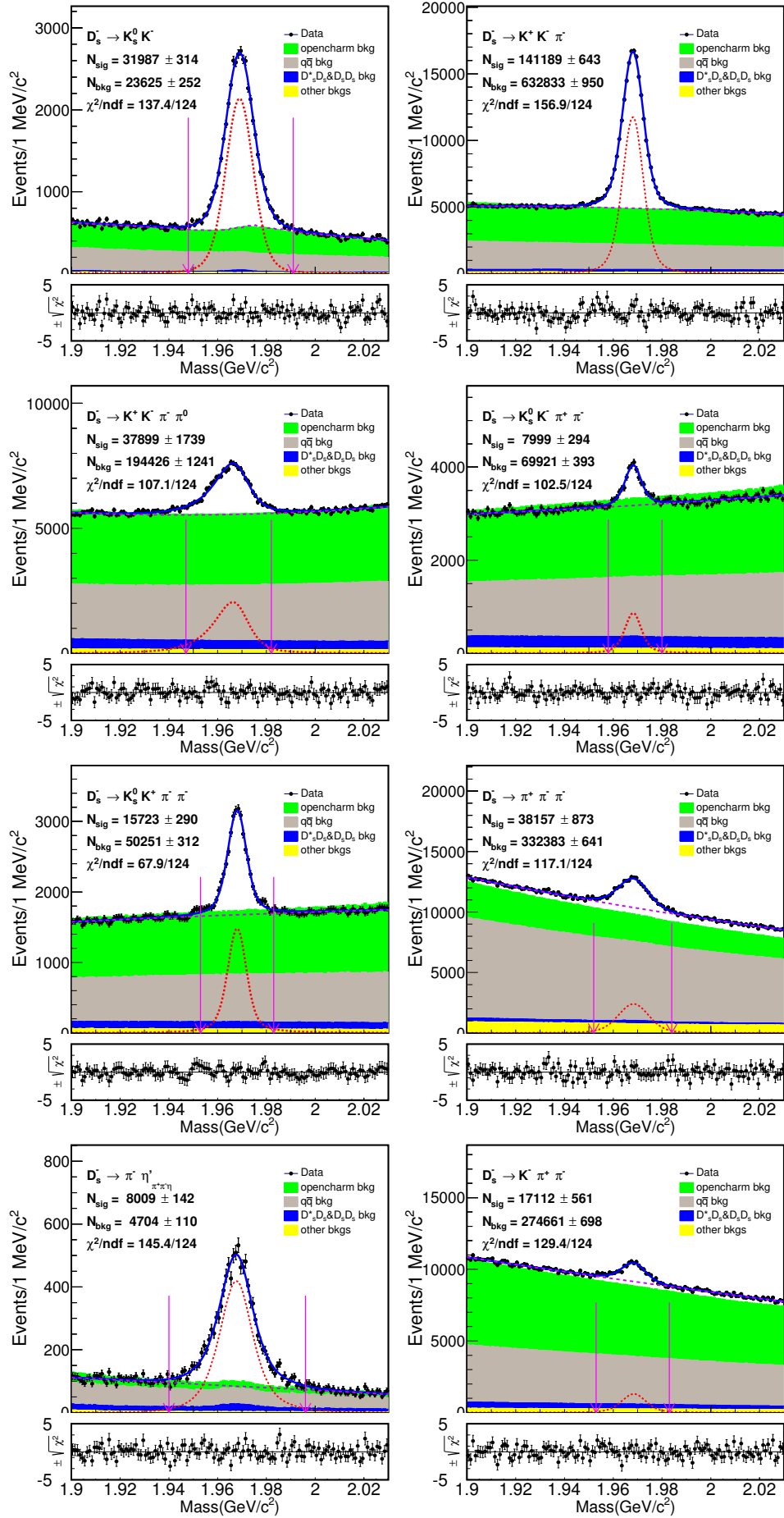
FIG. 10. Fits to the m_{tag} distributions of data. The points with error bars indicate data and the solid lines indicate the fit. Red short-dashed lines are signal, violet long-dashed lines are background. The region within the red arrows denotes the signal region.
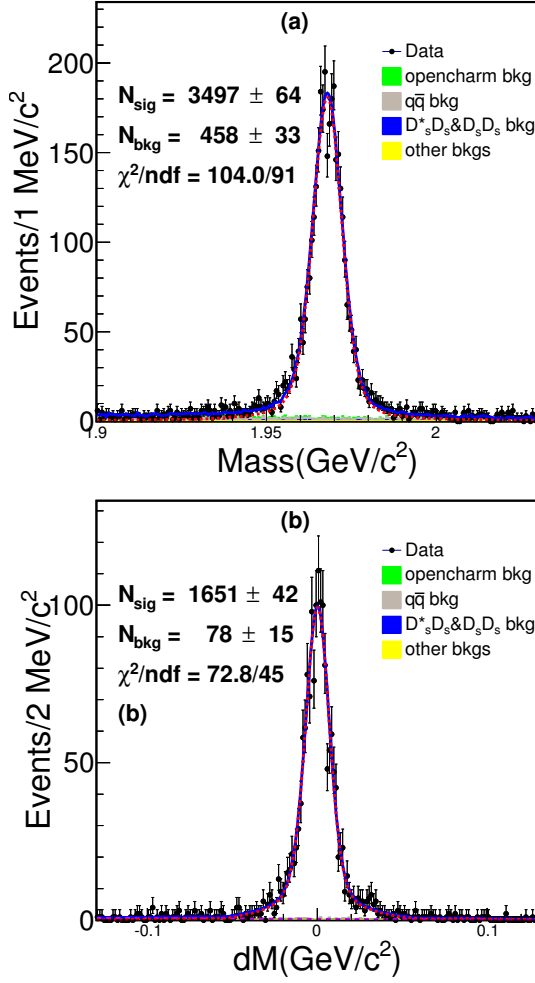
FIG. 11. Fit of (a)Cat. A and (b)Cat. B. We fit M_{sig} and dM for Cat. A and Cat. B, respectively. The signal shapes are the corresponding simulated shapes convoluted with a Gaussian function and the background shapes are described with second-order Chebychev polynomial.

signals for Cat. A and Cat. B, respectively; $\mathcal{B}_{tag}$ and $\mathcal{B}_{sig}$ are the branching fractions of a specific tag mode and the signal mode, respectively; ϵ_{tag} is the efficiency to reconstruct the tag mode; $\epsilon_{tag,sig}$ is the efficiency to reconstruct both the tag and signal decay modes.

Using the above equations, it's easy to obtain:

$$\mathcal{B}_{sig} = \frac{N_{sig}^{obsA} + 2N_{sig}^{obsB}}{\sum_{\alpha} Y_{ST}^{\alpha} \epsilon_{tag,sig}^{\alpha} / \epsilon_{tag}^{\alpha}}, \qquad (30)$$

where the yields N_{sig}^{obsA}, N_{sig}^{obsB} and Y_{ST}^{α} are obtained from data, while ϵ_{tag} and $\epsilon_{tag,sig}$ can be obtained from the appropriate MC samples, where α represents the tag modes.

C. Systematic Uncertainty

The following sources are taken in account to calculate systematic uncertainties.

- Uncertainty in the number of ST D_s^- candidates. We perform alternative fits with different background shapes, signal shapes and fit ranges to obtain the uncertainties related to the corresponding factors. We change the background shape from the second-order Chebychev polynomial to a third-order Chebychev polynomial and the relative change of branching fraction is 0.18%. The systematic in signal shape is determined to be 0.16% by performing an alternative fit without convoluting the Gaussian resolution function. For fit range, we vary the fit range from $[1.90, 2.03]$ GeV/c^2 to $[1.90, 2.02]$ GeV/c^2 and the relative difference of branching fraction is 0.24%. According to Table IX, the total ST yields of the eight tag modes is 298487 $\pm$ 2186. Then the uncertainty due to background fluctuation is $2186/298487 = 0.73\%$. The quadrature sum of these terms, that is the uncertainty in the number of ST D_s^- candidates, is 0.84%.

- Signal shape. The systematic uncertainty due to the signal shape is studied with the fit without the Gaussian function convoluted, the double tag yield shift is taken as the related effect.

- Background shape and fit range. For background shape and the fit range in the fit, the third-order Chebychev polynomial is used to replace the nominal ones and the fit range of $[1.90, 2.03]$ GeV/c^2 for Cat. A and $[-0.13, 0.13]$ GeV/c^2 for Cat. B are changed to $[1.90, 2.02]$ GeV/c^2 and $[-0.14, 0.14]$ GeV/c^2 respectively. The largest branching fraction shift is taken as the related effect.

- Fit bias. The possible bias is estimated by the input/output check using the round 30-40 of DIY MC, which is shown in Table XI. The estimated mean ($\mu_{\mathcal{B}}$) and its uncertainty (σ_{μ}) is calculated with the following formulas:

$$\mu_{\mathcal{B}} = \frac{\sum_i \frac{\mu_i}{\sigma_i^2}}{\sum_i \frac{1}{\sigma_i^2}}, \quad \sigma_{\mu}^2 = \sum_i \frac{1}{\sigma_i^2}, \qquad (31)$$

where μ_i and σ_i are the measured branching fraction value and its statistical uncertainty for the sample i. The combined result of the round 30-40 is $\mu_{\mathcal{B}} = (5.462 \pm 0.021)\%$. The relative change compared to the input value is 0.1%, which is very small and negligible.

- $K^{\pm}$ and $\pi^{\pm}$ Tracking/PID efficiency. Based on the works [18] and [19] by Xingyu Shan and Sanqiang Qu, etc. we find that it's enough to assign 1.1% ,

TABLE XI. Input/output check using the round 30-40 of DIY MC.

Round	$\mathcal{B}(D_s^+ \to K^+K^-\pi^+)(\%)$
31	5.562 ± 0.076
32	5.497 ± 0.076
33	5.407 ± 0.076
34	5.636 ± 0.078
35	5.490 ± 0.076
36	5.397 ± 0.076
37	5.369 ± 0.076
38	5.490 ± 0.077
39	5.353 ± 0.075
40	5.435 ± 0.076
Combined result	5.462 ± 0.021

0.4%, 1.1% and 0.2% as the systematic uncertainty for $K^\pm$ PID, $\pi^\pm$ PID, $K^\pm$ tracking, $\pi^\pm$ tracking efficiencies, respectively.

- MC statistics. The uncertainty of MC statistics is obtained by $\sqrt{\sum_i f_i (\frac{\delta_{\epsilon_i}}{\epsilon_i})^2}$, where f_i is the tag yield fraction and ϵ_i is the signal efficiency of tag mode i.

- Dalitz model. The uncertainty from the Dalitz model is estimated as the change of efficiency when the Dalitz model parameters are varied by their uncertainties.

All of the systematic uncertainties mentioned above are summarized in Table XII and uncertainties in the table are relative shifts.

TABLE XII. Systematic uncertainties of branching fraction.

Source	Sys. Uncertainty (%)
Number of D_s^-	0.8
Signal shape	0.5
Background shape and fit range	0.9
$K^\pm$ and $\pi^\pm$ PID efficiency	1.5
$K^\pm$ and $\pi^\pm$ Tracking efficiency	1.3
MC statistics	0.2
Dalitz model	0.5
total	2.4

VII. CONCLUSION

This analysis presents the amplitude analysis of the decay $D_s^+ \to K^+K^-\pi^+$. Table XIII is a comparison of amplitude analysis between BABAR, CLEO-c and this analysis. Our results are roughly consistent with those of BABAR and CLEO-c. For the fit fraction of $D_s^+ \to$

$f_0(980)\pi^+/a_0(980)\pi^+$, we tend to agree with the result of BABAR.

In this analysis, as $a_0(980)$ and $f_0(980)$ overlap and parameters of $f_0(980)$ is not well measured, we have extracted the $\mathcal{S}$-wave lineshape in the low end of K^+K^- mass spectrum with the model independent method.

We also measure the branching fraction $\mathcal{B}(D_s^+ \to K^+K^-\pi^+) = (5.47 \pm 0.07_{stat.} \pm 0.13_{sys.})\%$. As is shown in Table XIV, the branching fraction of this analysis has the best precision.

We also obtained the branching fractions for the intermediate processes, listed in Table XV. According to $\mathcal{B}(D_s^+ \to a_0(980)\pi^+, a_0(980) \to \pi^0\eta)$ measured in the Ref. [4], we can obtain $\mathcal{B}(D_s^+ \to a_0(980)\pi^+, a_0(980) \to K^+K^-)$ is about 0.14%, which is much less than $\mathcal{B}(D_s^+ \to S(980)\pi^+)$ listed in Table XV. We can see that $\mathcal{B}(D_s^+ \to S(980)\pi^+)$ measured in this analysis is not inconsistent with the one obtained in the Dalitz plot analysis of $D_s^+ \to \pi^+\pi^0\eta$ [4]. With $\mathcal{B}(\bar{K}^*(892)^0 \to K^-\pi^+)$ and $\mathcal{B}(\phi(1020) \to K^+K^-)$ from PDG [12], we can obtain $\mathcal{B}(D_s^+ \to \bar{K}^*(892)^0 K^+) = (3.94 \pm 0.12)\%$ and $\mathcal{B}(D_s^+ \to \phi(1020)\pi^+) = (4.60 \pm 0.17)\%$. The comparison of $\mathcal{B}(D_s^+ \to \bar{K}^*(892)^0 K^+)$ and $\mathcal{B}(D_s^+ \to \phi(1020)\pi^+)$ between this analysis and some theory predictions [5] is listed in Table XVI. Our results are consistent with theory predictions based on solutions (A1), (S4) and (pole) listed in Table XVI.

VIII. APPENDIX A: AMPLITUDES TESTED

TABLE XIII. Comparison of fit fraction between BABAR, CLEO-c and this amplitude analysis.

Amplitude	BABAR	CLEO-c	This Analysis
$D_s^+ \to \bar{K}^*(892)^0 K^+$	47.9±0.5±0.5	47.4±1.5±0.4	48.3±0.9±0.6
$D_s^+ \to \phi(1020)\pi^+$	41.4±0.8±0.5	42.2±1.6±0.3	40.5±0.7±0.9
$D_s^+ \to S(980)\pi^+$	16.4±0.7±2.0	28.2±1.9±1.8	19.3±1.7±2.0
$D_s^+ \to \bar{K}_0^*(1430)^0 K^+$	2.4±0.3±1.0	3.9±0.5±0.5	3.0±0.6±0.5
$D_s^+ \to f_0(1710)\pi^+$	1.1±0.1±0.1	3.4±0.5±0.3	1.9±0.4±0.6
$D_s^+ \to f_0(1370)\pi^+$	1.1±0.1±0.2	4.3±0.6±0.5	1.2±0.4±0.2
$\sum FF(\%)$	110.2±0.6±2.0	129.5±4.4±2.0	114.2±1.7±2.3
χ^2/NDF	$\frac{2843}{2305-14}=1.2$	$\frac{178}{117}=1.5$	$\frac{290}{291-10-1}=1.04$
Events	96307 ± 369(purity 95%)	14400(purity 85%)	4381(purity 99.6%)

TABLE XIV. Comparisons of branching fraction between BABAR, CLEO-c and this analysis.

$\mathcal{B}\ (D_s^+ \to K^+ K^- \pi^+)(\%)$	Collaboration
$5.55 \pm 0.14_{stat.} \pm 0.13_{sys.}$	CLEO-c [24]
$5.06 \pm 0.15_{stat.} \pm 0.21_{sys.}$	BELLE [25]
$5.78 \pm 0.20_{stat.} \pm 0.30_{sys.}$	BABAR [26]
$5.47 \pm 0.08_{stat.} \pm 0.13_{sys.}$	BESIII(this analysis)

TABLE XV. The branching fractions measured in this analysis.

Process	Branching fractions (%)
$D_s^+ \to \bar{K}^*(892)^0 K^+,\ \bar{K}^*(892)^0 \to K^- \pi^+$	$2.64\ \pm\ 0.06_{stat.}\ \pm\ 0.07_{sys.}$
$D_s^+ \to \phi(1020)\pi^+,\ \phi(1020) \to K^+ K^-$	$2.21\ \pm\ 0.05_{stat.}\ \pm\ 0.07_{sys.}$
$D_s^+ \to S(980)\pi^+,\ S(980) \to K^+ K^-$	$1.05\ \pm\ 0.04_{stat.}\ \pm\ 0.06_{sys.}$
$D_s^+ \to \bar{K}_0^*(1430)^0 K^+,\ \bar{K}_0^*(1430)^0 \to K^- \pi^+$	$0.16\ \pm\ 0.03_{stat.}\ \pm\ 0.03_{sys.}$
$D_s^+ \to f_0(1710)\pi^+,\ f_0(1710) \to K^+ K^-$	$0.10\ \pm\ 0.02_{stat.}\ \pm\ 0.03_{sys.}$
$D_s^+ \to f_0(1370)\pi^+,\ f_0(1370) \to K^+ K^-$	$0.07\ \pm\ 0.02_{stat.}\ \pm\ 0.01_{sys.}$
$D_s^+ \to K^+ K^- \pi^+$ total branching fraction	$5.47\ \pm\ 0.08_{stat.}\ \pm\ 0.13_{sys.}$

TABLE XVI. The comparison of $\mathcal{B}(D_s^+ \to \bar{K}^*(892)^0 K^+)$ and $\mathcal{B}(D_s^+ \to \phi(1020)\pi^+)$ between this analysis and some theory predictions. $\mathcal{B}(exp)$ is the corresponding result of this analysis. $\mathcal{B}(A1)$, $\mathcal{B}(S4)$, $\mathcal{B}(pole)$ and $\mathcal{B}(FAT[mix])$ are theory predictions [5].

Mode	$\mathcal{B}(exp)$ (%)	$\mathcal{B}(A1)$ (%)	$\mathcal{B}(S4)$ (%)	$\mathcal{B}(pole)$ (%)	$\mathcal{B}(FAT[mix])$ (%)
$D_s^+ \to \bar{K}^*(892)^0 K^+$	3.97 ± 0.14	3.92 ± 1.13	3.93 ± 1.10	4.2 ± 1.7	4.07
$D_s^+ \to \phi(1020)\pi^+$	4.50 ± 0.18	4.49 ± 0.40	4.51 ± 0.43	4.3 ± 0.6	3.4

[1] P. L. Frabetti *et. al.* (E687 Collaboration), Phys. Lett. B **351**, 591 (1995).

[2] R. E. Mitchell *et. al.* (CLEO Collaboration), Phys. Rev. D **79**, 072008 (2009).

[3] P. del Amo Sanchez *et. al.* (BARBAR Collaboration), Phys. Rev. D **83**, 052001 (2011).

[4] M. Ablikim *et. al.* (BESIII Collaboration), Phys. Rev. Lett **123**, 112001 (2019).

[5] H. Y. Cheng, C. W. Chiang and A. L. Kuo, Phys. Rev. D **93**, 114010 (2016).

[6] M. Ablikim *et al.* (BESIII Collaboration), Nucl. Instrum. Meth. A **614**, 345 (2010).

[7] C. Zhang for BEPC & BEPCII Teams, Performance of the BEPC and the progress of the BEPCII, in: Proceeding of APAC, 2004, pp. 15-19, Gyeongju, Korea.

[8] S. Agostinelli *et al.* [GEANT4 Collaboration], Nucl. Instrum. Meth. A **506**, 250 (2003).

[9] R. G. Ping, Chin. Phys. C **38**, 083001 (2014).

[10] S. Jadach, B. F. L. Ward and Z. Was, Phys. Rev. D **63**, 113009 (2001).

[11] E. Richter-Was, Phys. Rev. D **62**, 034003 (2000).

[12] M. Tanabashi *et al.* (Particle Data Group), Phys. Rev. D, **98**, 030001 (2018).

[13] D. J. Lange, Nucl. Instrum. Meth. A **462**, 152 (2001); R. G. Ping, Chin. Phys. C **32**, 599 (2008).

[14] A. Hocker *et al.*, TMVA - Toolkit for Multivariable Data Analysis, PoS ACAT, (2007), arXiv:physics/0783039.

[15] J. C. Chen, G. S. Huang, X. R. Qi, D. H. Zhang and Y. S. Zhu, Phys. Rev. D **62**, 034003 (2000); R. L. Yang, R. G. Ping and H. Chen, Chin. Phys. Lett. **31**, 061301 (2014).

[16] S. U. Chung, Phys. Rev. D **56**, 7299 (1997).

[17] Sifan Zhang and Hailong Ma, BESIII DocDB 630-v35.

[18] https://indico.ihep.ac.cn/event/8006/contribution/1/material/slides/0.pdf

[19] https://indico.ihep.ac.cn/event/8023/contribution/1/material/slides/0.pdf

[20] B. S. Zou and D. V. Bugg, Eur. Phys. J. A **16**, 537 (2003).

[21] M. Alblikim *et. al.* (BESIII Collaboration), Phys. Lett. B **607** 243 (2005).

[22] Yu Lu and Liaoyuan Dong, BESIII DocDB 416-v30.

[23] G. Bonvicini *et. al.* (CLEO Collaboration), Phys. Rev. D **78**, 052001 (2001).

[24] P. U. E. Onyisi *et. al.* (CLEO Collaboration), Phys. Rev. D **88**, 032009 (2013).

[25] A. Zupanc *et. al.* (BELLE Collaboration), JHEP **1309**, 139 (2013).

[26] P. del Amo Sanchez *et. al.* (BABAR Collaboration), Phys. Rev. D **82**, 091003 (2010).

[27] M. Alblikim *et. al.* (BESIII Collaboration), Phys. Rev. D **95** 072001 (2017).